NASA TN D-228

TECHNICAL NOTE
D-228

FIXED-BASE SIMULATION STUDY OF A PILOT'S ABILITY TO CONTROL A WINGED-SATELLITE VEHICLE DURING HIGH-DRAG VARIABLE-LIFT ENTRIES

By John M. Eggleston, Sheldon Baron,
and Donald C. Cheatham

Langley Research Center
Langley Field, Va.

NATIONAL AERONAUTICS AND SPACE ADMINISTRATION

WASHINGTON April 1960

NATIONAL AERONAUTICS AND SPACE ADMINISTRATION

TECHNICAL NOTE D-228

FIXED-BASE SIMULATION STUDY OF A PILOT'S ABILITY TO CONTROL A WINGED-SATELLITE VEHICLE DURING HIGH-DRAG VARIABLE-LIFT ENTRIES

By John M. Eggleston, Sheldon Baron,
and Donald C. Cheatham

SUMMARY

A winged-satellite vehicle which enters the atmosphere at high (approaching 90°) angles of attack was simulated in five degrees of freedom by using a fixed-base simulator. The task of controlling the vehicle and the vehicle's trajectory during the entry was performed by a human pilot.

The tests showed that a pilot can successfully control the trajectory of the vehicle in several ways. A desired value of deceleration or rate of descent may be established and maintained. For entry angles up to -3°, the deceleration could be held between 3g and 4g. At entry angles of -6°, the pilot was able to limit the maximum deceleration between 7g and 8g.

Systematic changes in the damping and static stability of the vehicle were made to determine the sensitivity of these variables. Inadvertent coupling of the pitch- and roll-control motions by the pilot was noted when using a grip-type side-arm controller. Replacing this controller with a finger-tip side-arm controller eliminated the inadvertent coupling and made it possible for the pilot to fly simulated entries with zero damping of the vehicle's angular motions.

Lack of static stability in yaw for this vehicle was found to be objectionable. Adverse aerodynamic-control moment coupling was simulated. Such control coupling was considered undesirable but pilots could adapt themselves to control the vehicle even with extremely large amounts of coupling provided the vehicle was well damped.

INTRODUCTION

Several types of vehicles which are intended to return from orbiting flight about the earth have been proposed. Some of these vehicles glide

back to earth at small flight-path angles and thereby present a problem of heat protection for long periods of time but do not experience high decelerations. Other vehicles enter the atmosphere at a high drag condition which minimizes the heat-transfer problem but exposes the pilot to moderately high decelerations for a period of several minutes. With all of these vehicles there exists the problem of determining the stability, control, and the general handling characteristics necessary for piloted entries into the earth's atmosphere. The capabilities and limitations of human pilots to fly prescribed trajectories and to control the angular motions of these vehicles even at conditions of low stability are of particular interest. Since orbiting and atmospheric entries represent a rather large step from the flight conditions of current aircraft, a large part of the research must be done by realistic simulation of the pilot's tasks and flight conditions and, where possible, also the proper flight environment (that is, deceleration, heating, and mental state of the pilot). L 8 0 8

This paper covers the initial phase of a program to determine the pilot's ability to control the simulated trajectories and angular motions of satellite vehicles during high-drag variable-lift entries into the earth's atmosphere. The tests reported herein were made on a fixed-base (static) simulator in conjunction with an electronic analog computer located at the Langley Research Center. The vehicle simulated is representative of the high-drag variable-lift class of satellites which enter the atmosphere at small entry angles (1° to 6°) and require relatively short periods of time (4 to 8 minutes) to accomplish the entry. The details of the concept of this type of vehicle are reported in reference 1. Such vehicles have adequate capability of trajectory control (ref. 2) and a large range of static stability about the trim point (ref. 3). This preliminary study was made to determine regions of interest in the stability and control characteristics of such vehicles and to determine the pilots' abilities to control their trajectories with this class of vehicle. Some of the considerations shown by this investigation to be important in a simulation of satellite vehicles such as instrument display, pilot's controls, and analog-computer validation are documented.

SYMBOLS

a_n component of acceleration measured along negative Z body axis of vehicle

a_x component of acceleration measured along positive X body axis of vehicle

b reference span

$\bar{c}$	reference chord
C_c	chordwise force coefficient, positive along negative X body axis
C_l	rolling-moment coefficient measured about X body axis, $M_X/\bar{q}Sb$
C_m	pitching-moment coefficient measured about Y body axis, $M_Y/\bar{q}S\bar{c}$
C_n	yawing-moment coefficient measured about Z body axis, $M_Z/\bar{q}Sb$
C_N	normal-force coefficient positive along negative Z body axis
g	gravitational constant, 32.2 ft/sec^2
$\sqrt{gr'}$	circular satellite velocity at radial distance r', treated as a constant of 25,863 ft/sec
h	altitude
I_X, I_Y, I_Z	moments of inertia about principal body axes
$K_1, K_2, K_3 \ldots K_6$	constants
M_X, M_Y, M_Z	rolling, pitching, and yawing moments measured about X-, Y-, and Z-axes, respectively
M'	Mach number
L/D	ratio of lift force to drag force
p,q,r	angular velocities about X-, Y-, and Z-axes, respectively
$\bar{q}$	dynamic pressure
r'	radial distance from center of earth
P_n	undamped natural period, sec
T	time constant
S	wing area
t	time

$\bar{u} = V/\sqrt{gr'}$

V	velocity
W	weight of vehicle
X,Y,Z	three principal body axes (see fig. 2)
α	angle of attack
α_d	desired angle of attack
α_t	trim angle of attack
β	angle of sideslip
γ	flight-path angle
γ_o	entry or initial flight-path angle
δ	angle between velocity vector and reference horizon
$\delta_1,\delta_2,\delta_3$	roll-, pitch-, and yaw-control deflection, respectively
ϵ	angle-of-attack error, $\alpha - \alpha_d$
Θ	angle between reference and local horizon, $\gamma - \delta$
θ	pitch angle (see fig. 2)
ρ	atmospheric density
ϕ	roll angle
ψ	yaw angle
ζ	damping ratio, percent of critical damping
C_{l_ϕ}, C_{m_α}, and so forth	partial derivative of coefficient with respect to lower subscript; for example, $C_{l_\phi} = \frac{\partial C_l}{\partial \phi}$

Subscripts:

o	initial condition
max	maximum

Dot over a quantity denotes differentiation with respect to time.

DESCRIPTION OF SIMULATION

General

The static simulation of a satellite vehicle during an atmospheric entry was performed on the fixed-base cockpit mockup shown in figure 1. The vehicle simulated for these tests was a winged-satellite vehicle which entered the atmosphere at its zero-lift ($\alpha = 90^\circ$) condition. The concept of such a vehicle is described in reference 1. By varying the angle of attack and hence the lift, the pilot was able to control his trajectory. The details of this trajectory-control concept are given in reference 2. The trajectory (force) equations and the moment equations of the vehicle were simulated by using analog computer equipment located at the Langley Research Center. The cockpit simulator was located in the room with the computer equipment and connected directly to this equipment through electrical cables. The moments of inertia, weight, and dimensions for the winged vehicle (based on the concept of ref. 1) are given in table I.

Trajectory and Moment Equations

The winged-satellite vehicle was simulated with five degrees of freedom: longitudinal motions along and normal to the flight path and angular motions about the three principal axes of inertia of the vehicle. The lateral (side force) trajectory equation was not included since two of the effects, namely, lateral deviation of the trajectory and lateral accelerations on the pilot, were not important in the static simulator program. They would, of course, be important in navigation or centrifuge simulation. The third effect, namely, static stability in roll, is included in the simulation by including a term $C_{l_\beta}\beta = C_{l_\phi}\phi \sin \alpha$ in the rolling-moment equation. The five equations of motion describing the five degrees of freedom together with some auxiliary equations are given in appendix A and the sign convention is shown in figure 2. Derivation of the two force equations in terms of accelerations may be found

in reference 2. Curvature of the earth is taken into account but variations in gravity and the radial distance from the vehicle to the center of the earth (r') are neglected in calculating the centrifugal acceleration and the acceleration of gravity. Since the vehicle simulated presents essentially a flat surface at a large angle (60° to 110°) to the flight path, it was assumed that the resultant aerodynamic force acted normal to the surface at all times. Hence, there is no chordwise (along the X-axis) aerodynamic force ($a_X \propto C_c = 0$).

Euler Angle Relations

The conventional aircraft Euler angles are obtained by integrating:

$$\dot{\phi} = p + (r \cos \phi + q \sin \phi)\tan \theta$$

$$\dot{\theta} = q \cos \phi - r \sin \phi$$

$$\dot{\psi} = (r \cos \phi + q \sin \phi)\sec \theta$$

It can be seen that these equations become indeterminate when $\theta = 90^\circ$. This difficulty can be overcome either by redefining the reference axes and, consequently, the angle θ so that $|\theta| < 90^\circ$ during the tests or by redefining the order in which Euler rotations are taken. In this paper, the latter method is chosen.

The conventional Euler displacements are obtained by successively yawing, pitching, and rolling the vehicle about its successive Z-, Y-, and X-axes. In order that the new Euler relations be independent of θ, it is required that the order of rotation be first about the Y-axis through the angle θ. The next rotation is about the new X-axis through the angle ϕ. The final rotation is about the Z-axis through the angle ψ. With this order of rotation the relationship between angular velocities in body-fixed axes and earth-fixed axes becomes

$$\dot{\phi} = p \cos \psi - q \sin \psi$$

$$\dot{\theta} = (q \cos \psi + p \sin \psi)\sec \phi$$

$$\dot{\psi} = r + (p \sin \psi + q \cos \psi)\tan \phi$$

Since the pilot's task for these tests was to hold roll and yaw displacements near zero, the small-angle assumption was applied to these equations and the angular displacements (for use on the pilot's display and the calculation of α and β) ϕ, θ, and ψ were actually obtained by integrating

$$\dot{\phi} = p - q\psi$$

$$\dot{\theta} = q + p\psi$$

$$\dot{\psi} = r + q\phi$$

Vehicle Parameters

Static stability.- Based on the data of reference 3, the static stability of the vehicle in pitch and roll was established. The simulation covered the $2.0 \leqq M' \leqq 26$ range, and throughout this range the static stability coefficients, C_{m_α} and C_{l_ϕ}, were assumed to be constant with Mach number; hence, the moments due to roll and angle of attack were varied only with the dynamic pressure. The vehicle had no inherent static stability in yaw at angles of attack near 90° and therefore C_{n_ψ} was considered to be zero.

Control effectiveness.- Based on the known static stability of the vehicle, the aerodynamic control effectiveness in pitch and roll was chosen so as to give the pilot steady-state values of

$$\Delta\phi = \pm 30^\circ$$

for $\delta_1 = \pm\delta_{1_{max}}$ and

$$\Delta\alpha = \pm 30^\circ$$

for $\delta_2 = \pm\delta_{2_{max}}$

Since the winged vehicle has no inherent static stability in yaw at angles of attack near 90°, this criterion was not applicable for determining the aerodynamic yaw control power. Because of the high angle of

attack, it was assumed that any aerodynamic control about the yaw axis would be only about one-fourth as effective as the pitch and roll control surfaces and, subject to pilot acceptance, this magnitude was incorporated. The numerical values for the "standard" aerodynamic-control derivatives are given in table I. The magnitude of the moment due to aerodynamic-control deflection was also assumed to vary with dynamic pressure only.

The vehicle was considered to be equipped with both aerodynamic and proportional reaction controls such that, when the pilot moved his control stick or pedals, the aerodynamic surface and the reaction control valve operated simultaneously to produce a moment in the desired direction. Both types of controls operated throughout the entire trajectory through the pilot's controller. The reaction controls produced the same moment at all flight conditions while the aerodynamic control moments were proportional to the dynamic pressure.

The effectiveness of these jet reaction controls was at first based on a proposed criterion that at a condition of zero dynamic pressure the initial instantaneous angular acceleration about each axis due to a maximum control step displacement should be

$$\dot{p}(t > 0) = 15^\circ \text{ per sec}^2 \qquad \left(\delta_1(t > 0) = \delta_{1_{max}}\right)$$

$$\dot{q}(t > 0) = 5^\circ \text{ per sec}^2 \qquad \left(\delta_2(t > 0) = \delta_{2_{max}}\right)$$

$$\dot{r}(t > 0) = 5^\circ \text{ per sec}^2 \qquad \left(\delta_3(t > 0) = \delta_{3_{max}}\right)$$

However, when the control characteristics were tested, the pilots commented that the reaction controls were much too sensitive at zero dynamic pressure and recommended a reduction of 75 percent in roll and 66 percent in pitch and yaw. These changes were incorporated before making the tests reported herein. The reaction-control coefficients as used in these tests are given in table I. The initial angular accelerations due to full control displacement are then

at $\delta_{1_{max}}$

$$\dot{p}(t > 0) = 3.73^\circ \text{ per sec}^2$$

at $\delta_{2_{max}}$

$$\dot{q}(t > 0) = 1.67^\circ \text{ per sec}^2$$

at $\delta_{3_{max}}$

$$\dot{r}(t > 0) = 1.67^{\circ} \text{ per sec}^2$$

Dynamic stability.- Damping was provided about all three axes. No distinction is made between how much of this damping is inherent and how much is provided by stability augmentation. However, it was assumed that

$$C_{l_p} = K_1 C_{l_{\delta_1}}$$

$$C_{m_q} = K_2 C_{m_{\delta_2}}$$

$$C_{n_r} = K_3 C_{n_{\delta_3}}$$

where K_1, K_2, and K_3 are constants determined from desired damping characteristics. Thus, the damping increases with dynamic pressure in the same way as control effectiveness. A schematic drawing of one channel of this simple pilot-damper-control relationship is shown in figure 3.

Prior to the tests the constants K_1, K_2, and K_3 were adjusted to give damping characteristics which the pilots considered acceptable for the task of flying entry trajectories. The variation of the damping ratio with dynamic pressure is shown in figures 4(a) and 4(b) for equivalent second-order systems in pitch and roll. The time constant for the equivalent first-order system in yawing velocity is shown in figure 4(c). (The equivalent second- and first-order systems are obtained by neglecting the aerodynamic and inertia coupling in each of the moment equations.) This acceptable level of stability is denoted on the figure as "standard" and reductions in the damping, made by successive reductions in the K values, are denoted as one-half, one-fourth, and one-eighth standard. The deceleration, related to the dynamic pressure through the relation

$$a_n = \frac{C_N}{W/S} \bar{q}$$

is also shown along the abscissa of figure 4 for the condition where $W/C_N S$ = 11.7 pounds per square foot.

At zero dynamic pressure, the static stability of the vehicle is zero about all three axes. The equivalent first-order time constants associated with rolling and pitching velocity at zero dynamic pressure are then 45 seconds and 75 seconds, respectively, for the values given in table I for C_{l_p} and C_{m_q}.

Aerodynamic-control coupling.- The effects of cross coupling due to aerodynamic control displacements were investigated. It is possible that the vehicle considered might have such coupling and some other proposed vehicles (for example, that of ref. 4) do exhibit rather strong cross coupling due to roll and yaw control displacements. For simplicity, such effects were included in an approximate (linear) way. In order to investigate such effects, it was assumed that a displacement of the aerodynamic roll control $(\delta_{l_{aero}})$ produced, in addition to a positive rolling moment, an equal but negative yawing moment and half as much negative pitching moment:

$$C_{l_{\delta_1}} = -C_{n_{\delta_1}} = -2C_{m_{\delta_1}}$$

The aerodynamic pitch control was assumed to produce only pitching moment:

$$C_{l_{\delta_2}} = C_{n_{\delta_2}} = 0$$

A positive displacement of the aerodynamic yaw control was assumed to produce a positive yawing moment, an equal but negative rolling moment, and half as much negative pitching moment:

$$C_{n_{\delta_3}} = -C_{l_{\delta_3}} = -2C_{m_{\delta_3}}$$

Actually, both favorable (such as positive yawing moment accompanied by positive rolling moment) and adverse (such as positive yawing moment accompanied by negative rolling moment) cross-control coupling were tried but, as the names suggest, the adverse coupling produced the more difficult control problem. Thus, for the tests reported herein, whenever cross aerodynamic control moments were produced, these moments were always adverse.

Description of Cockpit

General.- The layout of the simulated cockpit is shown in the photograph presented as figure 5(a). The photograph was taken from a position just behind the position where the pilot's head would be and shows the instrument display, the rudder pedals, and the side-arm controller located on the right. The pilot sits in the simulated cockpit in a normal upright position.

Instrument display.- The instrument display was intended to provide the pilot with information regarding the attitude and motion of the vehicle. The instrument panel includes both active instruments and dummy instruments. The active ones are grouped in the center portion of the panel in a modified T-arrangement and may be seen in better detail in figure 5(b). The dummy instruments were included merely to add some realism to the appearance of the panel. The active instruments are identified in figure 5(b) and include an attitude group consisting of a pitch- and roll-attitude indicator (generally referred to as an "eight-ball"), and meter-type instruments for yaw angle, sideslip angle, angle of attack, and angle-of-attack error. The trajectory variable instruments form a bar over the basic T formed by the attitude group and are made up of meter-type instruments indicating (from left to right): normal acceleration (a_n), rate of descent, altitude, and velocity. This instrument arrangement was determined from pilots' opinions in preliminary tests. In general, the arrangement was felt to be as satisfactory as could be obtained with conventional-type instruments. Some improvement could perhaps be obtained through the use of integrated-type displays such as those discussed in reference 5.

The angle-of-attack error indicator, located to the right of the attitude "eight-ball," requires some explanation. In reference 2 an automatic control was described which programed the angle of attack along the trajectory as a function of deceleration and rate of change of deceleration, namely,

$$\alpha_d = 90^\circ - K_4 a_n - K_5 \dot{a}_n$$

The purpose of varying the angle of attack in this manner was to establish and maintain a predesired value of deceleration throughout most of the entry as long as the entry angle was between 0° and -3°. With $K_4 = 4$ and $K_5 = 250$ the data of reference 2 showed that the deceleration could be controlled to the vicinity of 3g. For the present tests, an indicator which showed the difference between the actual angle of attack of the vehicle and the angle of attack computed from the above relationship was displayed to the pilot. Thus, this indicator shows the angle-of-attack error,

$$\epsilon = \alpha_{actual} - \alpha_{desired}$$

By utilizing this instrument and by keeping the error small, the pilot should be able to control the vehicle so that maximum decelerations between 3g and 4g would be obtained.

The attitude group of instruments were all mechanized to be "fly to" instruments, that is, if the yaw-angle indicator went to the right, a left rudder deflection was required for correction or if the angle-of-attack needle went up, a nose-down control motion was required for correction. This consistency was a good feature and the pilots were of the opinion that the same philosophy should also apply to the motion instruments which the pilot could control indirectly by appropriate change in attitude. For example, since decreasing angle of attack resulted in decreased deceleration, the deceleration instrument could have been more easily interpreted with regard to the control correction required had the indicator moved up for increasing g rather than down.

Cockpit controls.- The pilot's controls consisted of a set of conventional rudder pedals for yaw control and a side-located controller for pitch and roll control. Most of the tests were performed with a grip-type two axes side-located controller located at the end of the pilot's right arm rest. The controller can be seen in the bottom right of figure 5(a) and is shown in a side view in figure 5(c). This side-arm controller was designed to be mechanically linked to a hydraulic control system. Aileron deflection is obtained by rotating the hand grip laterally about a pivot axis which is located 2.85 inches below the hand grip. Elevator control is actuated by motions of the hand about a pivot axis which passes through the wrist. The controller was limited to $\pm 20^{\circ}$ lateral (aileron control) movement and about $\pm 30^{\circ}$ longitudinal (elevator control) movement. Control feel forces were provided by linear centering springs about both motion axes. There was no spring detent for positive centering; however, the friction forces were negligible. A pitch trim was installed on the top of the stick grip but was not wired for use during the tests.

In the latter stages of the reported tests the side-located controller just described was replaced with a small "finger-tip" control stick also located at the end of the pilot's arm rest. This controller, which can be seen in figure 5(d), consisted of a small shaft with a knob on the top. The knob was 3 inches above the roll-pitch pivot point and 1.5 inches above the top of the box. Designed for electronic control systems, the stick was spring loaded (approximately 2.5 pounds for full deflection) and had no intentional friction. The design was similar to the side-located controller reported in reference 6 which has been flight tested over a period of several years.

The rudder pedals which can be seen in figures 5(a) and 5(d) were provided for conventional control about the yaw axis and could be moved ±3 inches. Spring centering was used to provide light rudder control forces.

PROCEDURE

For most of the simulated entries, four basic tasks were given the pilots. These tasks were:

(1) Make step changes in angle of attack when the deceleration reaches a specified value.

(2) Hold constant or establish and maintain a specified rate of descent.

(3) Establish and maintain a specified value of deceleration.

(4) By using the angle-of-attack error indicator, vary the angle of attack as required to maintain a zero error in this indicator.

After the capability of a pilot to perform these tasks with acceptable vehicle dynamics and control effectiveness was established, one of the vehicle characteristics was varied during successive entries with the pilot given one of the four basic tasks. Varied in this manner were static and dynamic stability, reaction-control effectiveness, and aerodynamic-control moment coupling. Most of the entries were made with initial flight-path angles of -1° to -3° but one group of tests was made by arbitrarily setting the initial flight-path angle between -3° and -6°. Although this procedure was followed by several pilots in different orders of sequence, the results to be presented are those of only one pilot. The results are considered to be representative of an experienced pilot proficient in the operations of the simulator and in the proposed operations of the simulated vehicle.

RESULTS AND DISCUSSION

General

In all the trajectories to be discussed, several of the initial conditions were the same. The trajectories always were started at an altitude of 350,000 feet and at circular satellite velocity for which a value of 25,863 feet per second was used. The velocity is plotted in the nondimensional form $\bar{u} = V/25{,}863$ so that $\bar{u}$ starts at 1.0 and approaches

0.04 at the end of the entry. Entry angles covered a range from -1° to -6°. It may be helpful in studying the trajectories to note that, for the given initial value of velocity, the initial rate of descent is approximately equal to (450 feet per second) times (the entry angle in degrees). Thus a -3° entry angle represents an initial rate of descent of 1,350 feet per second.

Point Mass Trajectories

In reference 2 some trajectories were presented for a point mass (no moments about the center of gravity) having the same $W/C_N S$ as the vehicle considered here. The trajectories of reference 2 were calculated by using a digital computer whereas, for the tests of this paper, an analog computer operating in real time was employed. Since the trajectories of interest require up to 10 minutes, some validation of the trajectories obtained by the analog computer appeared to be justified. At the same time, the characteristics of these trajectories can be illustrated. In order to compare trajectories calculated by the two methods, a number of trajectories calculated on the digital computer were also obtained with the analog computer for the case where the vehicle was treated as a point mass. Two of these trajectories are shown in figure 6. In figure 6(a), the angle of attack was fixed at 90° which is the condition of zero lift and maximum drag. The entry angle γ_o was -1° and deceleration reached a maximum of 7g at just under 300 seconds. In figure 6(b), the angle of attack was held constant at 79° which represents an L/D of about 0.2. The entry angle was -3° and the deceleration reached 4.5g at 110 seconds.

In general, the agreement between the analog computed and digital computed trajectories of reference 2 was found to be good. (In order to achieve consistent trajectories, it was necessary to use as an initial condition $\dot{h}_o$ rather than γ_o since small errors in γ_o led to appreciable differences in the deceleration time history. See appendix B.) One difference in the calculations is noteworthy. In reference 2, an exponential fit to the ARDC atmosphere (ref. 7) was used whereas, for the trajectories reported here, density as a function of altitude was obtained directly from the ARDC model atmosphere. The primary difference in the trajectories appears to be a 12.5-percent reduction in the maximum value of deceleration when the ARDC model atmosphere is used. It can be shown (for example, ref. 2) that the maximum deceleration is directly dependent on the instantaneous density gradient rather than on the average; thus some differences in the calculated decelerations should be expected. Although the exact nature of the altitude-density variation in the upper atmosphere is still speculative, either model atmosphere should provide representative results. Therefore, except to note this difference, no further discussion appears to be justified here. Some discussion of the

more important problems experienced in the analog simulation of trajectory equations over extreme ranges of altitude and velocity is given in appendix B.

Piloted Entries With Standard Vehicle Dynamics

With the vehicle dynamics included and the stability derivatives set at their "standard" value (see table I), the pilot was given several tasks to perform during simulated entries. The trajectory and angular motions of the vehicle resulting from the performance of three of these tasks are shown in figure 7. During the simulated entry of figure 7(a), the pilot was instructed to first pulse his roll (δ_1) and pitch (δ_2) control and then to make a step reduction in angle of attack from 90° to 80° when the deceleration reached 2g. Although the angle-of-attack scale on the figure is so small as to make the change almost imperceptible, the step change was made and the deceleration reached a maximum of 3.5g.

Two factors that were found to be important during this investigation are illustrated in figure 7(a). The lack of static stability in yaw of this vehicle is apparent in the time histories of yaw angle ψ and of the displacement of pilot's yaw control δ_3. Given any perturbation, yaw would drift off until corrected by the pilot. The second factor was the cross-controlling characteristics of the pilot's side controller.* At about 205 seconds the pilot intentionally pulsed the pitch control. In doing so, the records show he inadvertently produced a roll signal (of the opposite sign) at the same time. At 220 seconds the pilot intentionally pulsed the roll control without disturbing the vehicle in pitch. Although the cross-control characteristic noted during the first pulse was not important at this condition of damping, its presence is noteworthy and its effect will be discussed later.

A second task performed by the pilot is illustrated by the time history of figure 7(b). For this entry the pilot was instructed to hold the vehicle's rate of descent constant as long as it was aerodynamically possible. The entry angle was -2°. This type of entry was investigated theoretically in reference 2 and the angle-of-attack requirements for constant-rate-of-descent trajectory for several entry angles are given in that reference. It can be seen that very little control is required for this task, but the normal deceleration reached 7g.

As discussed in the section on instruments, one of the display instruments consisted of a zero reader which showed any error between the angle of attack of the vehicle and an angle of attack calculated as

*There was no vehicle aerodynamic control moment coupling during the entries discussed here.

a function of deceleration. The calculated angle of attack was designed to produce a deceleration of about 3g. Figure 7(c) shows a time history of a piloted entry where the pilot was instructed to vary his angle of attack so as to maintain a zero error on this meter. The entry angle was -3°. The time history shows that the pilot kept the error ϵ small and that the deceleration stayed between 3.5g and 2.5g throughout most of the entry.

Coupling between the roll and pitch control deflections can again be observed at 190 seconds in figure 7(c). Note that the scale of the pitch control is one-half that of the roll control in this time history. This control deflection produced a 3° change in roll angle and a 2° change in pitch angle.

Variations in Damping

For a specified task and identical initial conditions, piloted entries were made with various levels of vehicle damping. From the level of damping referred to as "standard" in figure 4, the damping was reduced during consecutive entries in steps of one-half, one fourth, one-eighth, and zero. Damping was reduced about all three axes by simultaneous reductions in Cl_p, Cm_q, and Cn_r. Both aerodynamic and reaction control damping were affected by this reduction. Results are shown in figure 8 for five simulated entries made from a -1° entry angle. For all of these entries the pilot's task was to control angle of attack as indicated by any error on the zero reader.

In figure 8(a) the damping has been reduced to one-half the value illustrated in figure 7. About 75 seconds after the start of the entry, the pilot deliberately pulsed the pitch control and the time history shows the ensuing pitch-roll oscillation. Although it required some obvious effort on the part of the pilot, the magnitude of the oscillation was attenuated. At the time of the pulse the dynamic pressure was about 2 pounds per square foot. A roll-control pulse was applied at about 210 seconds ($\bar{q}$ = 16 pounds per square foot) and the roll oscillation damped to a small amplitude after several cycles.

In figure 8(b), the damping was 1/4 standard and the entry was made with only small oscillations in pitch and roll. The smoothness of these records, however, is deceptive. The pilot did not put in any intentional control disturbances since the corrections applied at the first of the entry indicated marginal stability. The neutral static stability in yaw is apparent although the vehicle exhibits a relatively low yaw drift rate.

The damping about all three axes was 1/8 standard in figure 8(c). During the first 245 seconds a residual oscillation in pitch and roll is present and the change in period with the change in dynamic pressure is

clearly evident. At about 245 seconds, the roll oscillation abruptly diverged. At this time the deceleration was 2.75g, the dynamic pressure was 32.2 pounds per square foot, and the period in pitch was 3.6 seconds, and the period in roll, 1.8 seconds. Entries at this condition of damping were attempted a number of times by several pilots and, in all cases, an abrupt roll or pitch-roll divergence occurred between 150 and 300 seconds. Another example of this is seen in figure 8(d) where the damping about all axes was zero.

A typical sequence of events leading up to this abrupt divergence can be seen most clearly in figure 8(c). Throughout most of the entry the pilot was attempting to damp out the roll oscillation, as seen in the record of δ_l. At about 245 seconds the pilot changed his technique and attempted to damp out the pitch oscillation. An abrupt forward (negative) motion of the stick produced a simultaneous stick deflection to the right (positive) and, when the stick was reversed, the pitch-roll stick deflections remained 180° out of phase. The pitch oscillation was held in check by the pilot but the vehicle immediately diverged in roll. In some cases when this coupling occurred, the pilots attempted to damp the rolling motion and both the pitch and roll oscillations diverged. Whatever technique was used, however, a divergence always occurred sometime during the first 300 seconds of the entry.

In order to ascertain how much effect the reaction control damping had on the pilots' ability to control the vehicle,* an entry was made with zero reaction-control damping and 1/4-standard aerodynamic-control damping. With the exception of reaction-control damping, all conditions were the same as the entry of figure 8(b). The result is shown in figure 8(e). It can be seen that the pilot was able to control the vehicle throughout the entry. The fluctuations in the zero reader error ϵ at the very end of this figure should be discounted. At conditions where γ approaches -90° and $\dot{V}$ approaches 0, the calculated angle of attack became very sensitive to noise and produced unreasonable fluctuation of the indicator. The pilots were instructed to ignore these fluctuations at the end of all runs in which this indicator was used.

Reaction-Control Effectiveness

During the initial phase of the entry, a transition in control effectiveness occurs as the principal source of control power shifts from the reaction controls to the aerodynamic controls. With the aerodynamic-control effectiveness fixed by the trim requirements (see section on control effectiveness), several levels of reaction-control effectiveness were investigated during simulated entries and the results are shown in figure 9. With an entry angle of -2° (a rate of descent of about 900 feet per second) the pilot was instructed to reduce his rate of descent to

*The aerodynamic-control power is equal to the reaction-control power in roll when $\bar{q}$ = 1/3 pound per square foot, in pitch when $\bar{q}$ = 0.6 pound per square foot, in yaw when $\bar{q}$ = 2.63 pounds per square foot.

450 feet per second and maintain that rate of descent as long as possible. The damping about all axes was "standard." (Since the reaction-control damping was assumed to be proportional to the reaction-control effectiveness, the stability augmentation gain was increased to compensate for each decrease in control effectiveness.) In figure 9(a), a complete time history is shown for a case where the reaction-control effectiveness was reduced to 1/2 standard (as given in table I). In figures 9(b) and 9(c), only the initial phase of two entries is shown where the reaction-control effectivenesses were, respectively, 1/4 and 1/8 standard. In figures 9(b) and 9(c) some rolling and pitching oscillations occurred during the transition which the pilot believed were caused by the change in response of the vehicle to his control displacements. Even for the simplified case considered where the control system had a perfect response, the lower values of reaction-control effectiveness were found to be barely adequate but not desirable.

L 8 0 8

Aerodynamic-Control Moment Coupling

A condition where the aerodynamic roll and yaw controls produced moments about all three principal axes was investigated. The magnitudes of aerodynamic control coupling used are described in the section "Vehicle Parameters" and hereinafter are referred to as standard control coupling. With standard damping, standard reaction control moments and standard aerodynamic control moments* with coupling, several simulated entries were made with a -3° entry angle. The pilot's task was to maintain a zero error on the angle-of-attack error indicator described previously. Two such entries are shown in figures 10(a) and 10(b). In both of these time histories a characteristic of coupled roll and yaw control moments can be seen. When the aerodynamic yaw control was applied to give a positive yawing moment this control deflection also caused a negative rolling moment. In order to compensate for this, the pilot applied a positive roll-control deflection but this deflection then caused, in addition to the positive rolling moment, an additional negative yawing moment. More positive yaw control was applied and the process continued with the pilot holding increasing amounts of positive roll- and positive yaw-control deflections. The process generally led to partial or total loss of control unless the pilot realized what was happening and compensated for it. An example of this condition can be

*One exception to the otherwise standard control effectiveness occurred at this point in the test program. Subsequent to the tests it was discovered that the computer gains for all the aerodynamic-control moments feeding into the pitch equation were inadvertently doubled during an overnight interruption. As a consequence, the pitch, roll, and yaw controls produced twice as much pitching moment as the standard coefficients would predict. This was the case for the runs shown in figures 10, 11, and 12.

seen at the start of the entry of figure 10(a) where the process continued up to about 70 seconds. The pilot stated he was unaware that he was holding a right roll deflection and that, as the dynamic pressure increased, he was forced to hold more and more right rudder deflection. (The aerodynamic roll control was about three times more powerful than the yaw control. See table I.) At about 65 seconds the pilot deliberately applied a nose-down step change in the pitch control. Because of the inertia coupling, this change produced a large negative yawing moment which the pilot unsuccessfully attempted to stop with a small rudder deflection. Full right rudder was applied and at 70 seconds a rather violent oscillation was started which the pilot was finally able to control.

The roll control was pulsed at about 285 seconds and the pilot made the proper yaw correction and no difficulty was experienced. (Note, however, the accompanying deflection of the pitch (δ_2) control.) At 360 seconds the pilot was told he was holding a right roll deflection (δ_1) and was told to release it. The reduction in corrective yaw control (δ_3) is very apparent.

Figure 10(b) shows the time history of an entry made at conditions identical to those of figure 10(a) except that no unnecessary control motions were applied. The trajectory and angular motions of the vehicle were smooth but the pilot continued to hold right-roll and right-yaw control deflections throughout the entry. Changes in pitch were made slower than usual and, as a consequence, the angle-of-attack error exceeded 10° on two occasions. Even with this error the maximum deceleration was only 3g.

The damping was reduced to 1/2 standard and, after several runs in which the pilot lost control of the vehicle, a successful entry was made and the data are shown in figure 10(c). On the unsuccessful attempts the records showed that the pilot, in attempting to damp a pitch oscillation, was inadvertently deflecting the controller in roll and the rolling and yawing moments caused a divergence about all three axes. An example of this effect is shown in figure 10(d) where the pitch control motions are almost perfectly reflected (pushing the stick forward caused the pilot to twist his wrist clockwise) by the roll control motions, the pitch deflections being five times larger in magnitude.

Variations in Static Stability

The static stability in roll and pitch was reduced to one-half the standard values both individually and jointly. Such changes did not significantly alter any of the results described in the preceding sections. With standard damping and standard aerodynamic-control coupling,

entries were made successfully with first the roll and then the pitch static stability reduced one-half. With both roll and pitch stability reduced one-half, one-eighth standard damping, and no control moment coupling, the pilot could not control the angular motions of the vehicle although the period of the oscillations were 1.414 times longer than for the case of standard static stability.

Variations in Piloting Tasks at Large Entry Angles

With standard stability, standard reaction controls, and standard (with the exception noted earlier) aerodynamic controls with 1/2-standard control moment coupling, several entries were made with initial flight-path (entry) angles up to -6°. In order to simulate failure of certain instruments, the pilot's instruments which displayed trajectory information were turned off except for one (or two) key instruments and the pilot was not informed as to the magnitude of the entry angle. He was told, however, of the limits, -1° to -6°.

L 8 0 8

Figure 11(a) shows an entry for which the initial flight-path angle was -3°. The pilot had only normal acceleration and angular displacements (θ, α, ϕ, ψ, β) displayed on his instrument panel and was instructed to establish and maintain a 3g deceleration throughout the entry. The records show that without knowledge of his entry angle (or rate of descent) the pilot employed large changes in angle of attack in order to accomplish the task. As a result, the deceleration was held to between $3\frac{1}{4}$g and $2\frac{1}{2}$g during the entry.

With the vehicle trimmed at an angle of attack of 60° the records show that the pilot was using about 40 percent of the available pitch control (about 10 percent of the required pitching moment was coming from the roll- and yaw-control deflections). The pilot was aware that some additional pitch control was available but limited the trim angle of attack to 60°.

In figure 11(b) the pilot's task and the initial flight conditions were the same as those of figure 11(a) except that the entry angle was -5°. The pilot's reaction to the rapid increase in deceleration was to reduce the angle of attack and to hold the maximum allowable lift (an L/D of about 0.5 is obtained at $\alpha = 60^\circ$) until after the deceleration reached its peak value of 6g. Since this value was twice the assigned value of 3g, the pilot attempted to reduce the deceleration slowly to the prescribed value. By the time the deceleration had reached 3g most of the kinetic energy of the vehicle had been dissipated.

The accelerometer was disconnected and the rate-of-descent indicator was connected for the entry shown in figure 11(c). The entry angle

was again -5° and the pilot's task was to establish and maintain a 450 feet per second rate of descent. The time history shows a high degree of success in accomplishing this task. The rate of descent was established at 450 feet per second and the maximum deceleration was 5.5g.

For the piloted entry of figure 11(d) the entry angle was -6°, the task was the same, and both rate of descent and deceleration were displayed to the pilot. (Altitude and velocity indicators were disconnected.) Good task and control proficiency was exhibited by the pilot but the deceleration reached 7.5g before the pilot could establish the desired rate of descent.

Side-located finger-tip controller.- In the foregoing tests made with a grip-type side-arm controller, it was noted in a number of cases that the pilot was cross-controlling inadvertently; that is, moderate to large deflections of the controller in pitch or roll were accompanied by smaller (1/5 to 1/4) deflections about the other axis. The cross-controlling or coupling was most prominent when an intentional deflection of the controller in pitch was accompanied by smaller unintentional deflections about the roll axis. In order to determine to what extent this coupling influenced the lowest level of vehicle damping that could be handled by the pilot, the grip controller was replaced with a side-located finger-tip controller described in the section on "Cockpit Controls." The conditions of the tests described in the section "Variations in Damping" were again set up and the tests repeated. The unintentional change in the aerodynamic-pitch-control effectiveness, noted earlier, was corrected and for both the original and the repeated tests the control effectiveness and static stability were standard.

With the finger-tip controller no cross-controlling occurred and the pilots were able to make simulated entries consistently at conditions of 1/8 standard and zero damping. Zero damping means that the moments which resist the angular velocities in roll, pitch, and yaw were set to zero. A negative lift-curve slope and a decrease in dynamic pressure are both destabilizing (see ref. 8), however, and can cause divergence of the vehicle in pitch and roll if these motions are not controlled. An entry made with the damping about all axes set to zero is shown in figure 12. The entry angle was -1° and the pilot's task was to maintain a zero error on the angle-of-attack error indicator. Small oscillations occurred in pitch and roll which the pilot did not attempt to damp. Usually these oscillations converged when the dynamic pressure increased and diverged when the dynamic pressure decreased. (This dynamic instability is proportional to $d\bar{q}/dt$. See ref. 8.) As long as the rate of divergence was gradual and the amplitude of the oscillation was small, the pilot generally did not attempt to damp either pitch or roll. When necessary, however, energy could be extracted from the oscillation with quick pulses of the roll or pitch control.

Comparison of controllers.- The two controllers used in these tests had several characteristics in common: spring loading, no breakout force, no intentional damping, and both were designed for use at moderate to high vehicle accelerations such as encountered during atmospheric entries. Principal differences, however, are found in the inertia and grip of the two controls. The grip-type controller similar to the controller designed for an NASA-AF-Navy hypersonic research airplane, had a relatively large inertia about its hinge points. The pilot gripped a handle similar to those mounted on the center stick of most aircraft. The finger-tip controller was a small pencil-shaped control stick that the pilot held with his finger tips and had low inertia.

From the characteristics of coupling in the grip-type controller, it appeared that the pilot in displacing the controller in pitch also twisted his wrist to produce roll. A forward motion generally caused a twist to the right and a rearward motion generally produced a left twist. However, on a few occasions the record shows the opposite trend.

Experience has shown that such characteristics can generally be corrected with a finite breakout force from trim. Since similar coupling characteristics at conditions of low damping were noted by pilots who participated in the static and dynamic simulation of the hypersonic research vehicle, a further study of the controller used in the research vehicle would appear to be warranted.

CONCLUSIONS

A winged satellite vehicle which enters the atmosphere at high (approaching 90°) angles of attack was simulated in five degrees of freedom using a fixed-base simulator. The task of controlling the vehicle and the vehicle's trajectory during the entry was performed by a human pilot. Although several pilots were used in the tests, the data presented are for simulated entries made by one pilot. Environmental conditions such as deceleration and cockpit temperature were not simulated. The purpose of these tests was to determine what factors were important to the pilot's control of the vehicle and the vehicle's trajectory during an atmospheric entry and what were the pilot's limitations. Different levels of static stability, damping, control effectiveness and aerodynamic-control moment coupling were investigated. The pilot was required to fly several different types of trajectories with entry angles between -1° and -6°.

1. The tests show that, given a display with sufficient trajectory information, a human pilot can successfully control his trajectory in a variety of ways. A desired value of deceleration or rate of descent may be established and maintained throughout most of the trajectory. Variations of angle of attack computed as a function of the deceleration

and displayed to the pilot can be followed by the pilot. As a result, for entry angles between 0° and -3°, the deceleration could be held to between 3g and 4g. At entry angles of -6° the pilot was able to limit the maximum deceleration to between 7g and 8g.

2. With acceptable damping, moderate changes in vehicle static stability from values obtained from wind-tunnel tests produced no detectable effect on the pilot's ability to control the vehicle. However, with standard static stability in pitch and roll, systematic reductions in the damping of the vehicle about all three axes indicated that for low values of roll and pitch damping (percent of critical damping never exceeds 0.1), the vehicle could not be controlled. The data indicated that, with the side-arm controller used for these tests, the pilot was inadvertently coupling his pitch and roll control motions. When this controller was replaced with a different side-arm controller, no such difficulties were experienced and the pilot was able to control the vehicle at zero damping about all three axes. Although no modification to the original controller was tested, experience has shown that small "breakout" forces can reduce or even eliminate such characteristics.

3. For the winged vehicle investigated, the lack of static stability in yaw was found to be objectionable and required the continuous attention of the pilot. If, in addition to the control of the vehicle, the pilot must perform some additional task such as navigation, it would appear advisable to provide the vehicle with artificial yaw static stability.

4. Conditions were simulated where the pilot's displacement of either the aerodynamic roll or yaw control surfaces produced proportional moments about all three body axes. Preliminary tests showed that adverse control moment coupling was more difficult to control than favorable control moment coupling, but either form was found to be objectionable. With practice, this vehicle could be controlled even with large amounts of (linear) control coupling, provided the vehicle also had good damping.

Langley Research Center,
National Aeronautics and Space Administration,
Langley Field, Va., November 19, 1959.

APPENDIX A

EQUATIONS OF MOTION OF A SATELLITE VEHICLE DURING REENTRY FOR α_{trim} NEAR 90°

The equations of motion of a satellite vehicle during reentry with α_{trim} near 90° are as follows:

Force:

$$\frac{\dot{V}}{g} = -\left(a_n \sin \alpha - a_x \cos \alpha\right) - \sin \gamma$$

$$\frac{\dot{V}\gamma}{g} = \left(a_n \cos \alpha + a_x \sin \alpha\right) + \left(\frac{V^2}{gr'} - 1\right)\cos \gamma$$

Moment:

$$\dot{p} - \left(\frac{I_Y - I_Z}{I_X}\right)qr = \frac{\bar{q}Sb}{I_X}\left(C_{l_p}p + C_{l_\phi}\phi \sin \alpha + C_{l_{\delta_1}}\delta_1 + C_{l_{\delta_3}}\delta_3\right)$$

$$\dot{q} - \left(\frac{I_Z - I_X}{I_Y}\right)pr = \frac{\bar{q}S\bar{c}}{I_Y}\left(C_{m_q}q + C_{m_\alpha}\Delta\alpha + C_{m_{\delta_2}}\delta_2 + C_{m_{\delta_1}}\delta_1 + C_{m_{\delta_3}}\delta_3\right)$$

$$\dot{r} - \left(\frac{I_X - I_Y}{I_Z}\right)pq = \frac{\bar{q}Sb}{I_Z}\left(C_{n_r}r + C_{n_{\delta_3}}\delta_3 + C_{n_{\delta_1}}\delta_1\right)$$

Euler angle approximations:

$$\dot{\phi} = p - q\psi$$

$$\dot{\theta} = q + p\psi$$

$$\dot{\psi} = r + q\phi$$

Auxiliary relationships:

$$\dot{h} = V \sin \gamma \qquad a_n = \frac{C_N}{W/S} \bar{q}$$

$$\text{Range} \approx \int_0^t V \cos \gamma \, dt \qquad -a_x = \frac{C_c}{W/S} \bar{q}$$

$$\alpha + \gamma = \theta \qquad \Delta\alpha = \alpha - \alpha_t$$

APPENDIX B

SOME PROBLEMS INHERENT TO THE ANALOG SIMULATION OF TRAJECTORIES

Two general problems of interest were studied during the analog simulation of atmospheric entries. The first of these was to choose a suitable method for the generation of dynamic pressure. The altitude range to be considered was from 50,000 feet to 350,000 feet. Over this range of altitude, the density ρ varies through a ratio of 10^6:1. The velocity has a variation, starting at orbital velocity, of approximately 25:1. Hence, the square of the velocity has a ratio of variation of about 625:1. During an entry the product of these two variables is such that the dynamic pressure varies from about 0 to 100. The density variation must be simulated on the computer by some type of nonlinear function generator. It can be seen that, if a scale factor is chosen to give a 100 volts for the maximum value of density, 3×10^{-4} at $h = 50{,}000$ feet, any values less than 3×10^{-6}, or from 155,000 feet upward, would correspond to machine voltages of less than 1 volt. For these values the signal-to-noise ratio becomes significant and the function is subject to large errors. Therefore, for most of the run the density would be essentially meaningless.

In order to overcome this problem, $\rho^{1/6}$ was generated and the dynamic pressure was arrived at through successive multiplications, as shown in the following sketch:

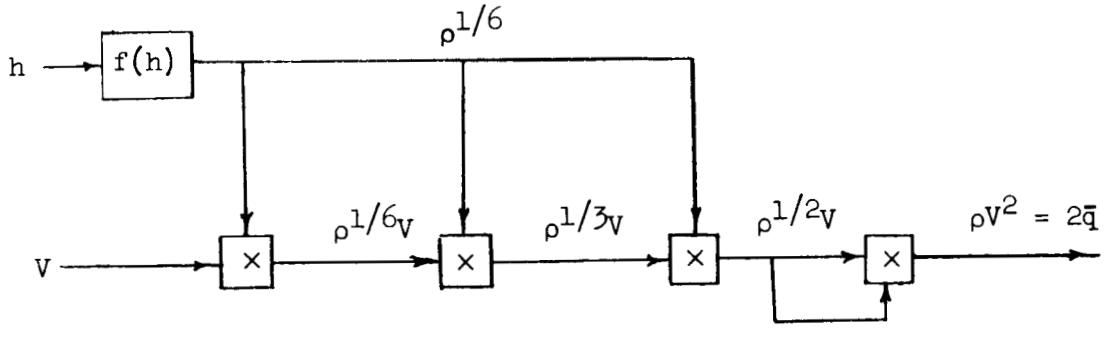

Nowhere in the simulation did ρ or V^2 appear by themselves. Since the sixth root of ρ has a ratio of variation of only 10:1, the function generator remained in the meaningful voltage range for the entire altitude range. It was realized that any errors in the function itself

would be amplified by the successive multiplications and it was of utmost importance to generate the function as accurately as possible. Consequently, tapped potentiometers were used for the generation of the sixth root of ρ. They were chosen for their high accuracy and for their minimum drift characteristics. The results demonstrate the successful generation of dynamic pressure by this method.

The other problem was encountered in attempts to compare trajectories obtained from the analog computer with those obtained from a digital machine. It was noted that, when attempts were made to check a trajectory for an initial entry angle of -3° and a constant angle of attack of 79°, the initial portion of the acceleration time history was very difficult to repeat. However, the peak acceleration was almost identical in all cases. This failure to repeat the answers was traced to an inability to set the entry angle accurately enough. In order to verify this conclusion the digital setup was used to calculate a trajectory with the same angle of attack but with an entry angle of -2.9°. The acceleration time histories for the two trajectories are shown in figure 13. The two trajectories show a marked difference in the early part of the acceleration profile but the peak values are very nearly equal.

A difference of 0.1° of entry angle represented only a 0.05-percent error in the analog computer and this error is well within the tolerances to be expected. An improvement in repeatability was obtained with fine adjustments of the initial flight-path (entry) angle such that the initial rate of descent was the correct value. It is believed that the differences encountered were not of a nature to in any way invalidate the conclusions obtained.

REFERENCES

1. Staff of Langley Flight Research Division (Compiled by Donald C. Cheatham): A Concept of a Manned Satellite Reentry Which is Completed With a Glide Landing. NASA TM X-226, 1959.

2. Eggleston, John M., and Young, John W.: Trajectory Control for Vehicles Entering the Earth's Atmosphere at Small Flight-Path Angles. NASA MEMO 1-19-59L, 1959.

3. Penland, Jim A., and Armstrong, William O.: Static Longitudinal Aerodynamic Characteristics of Several Wing and Blunt-Body Shapes Applicable for Use As Reentry Configurations at a Mach Number of 6.8 and Angles of Attack up to 90°. NASA TM X-65, 1959.

4. Eggers, Alfred J., Jr., and Wong, Thomas J.: Re-Entry and Recovery of Near-Earth Satellites, With Particular Attention to a Manned Vehicle. NASA MEMO 10-2-58A, 1958.

5. Svimonoff, Constantine: The Air Force Integrated Flight Instrument Panel. WADC Tech. Rep. 58-431, ASTIA Doc. 155788, U.S. Air Force, Oct. 1958.

6. Sjoberg, S. A., Russell, Walter R., and Alford, William L.: Flight Investigation of a Small Side-Located Control Stick Used With Electronic Control Systems in a Fighter Airplane. NACA RM L56L28a, 1957.

7. Minzner, R. A., and Ripley, W. S.: The ARDC Model Atmosphere, 1956. Air Force Surveys in Geophysics No. 86 (AFCRC TN-56-204, ASTIA Doc. 110233), Air Force Cambridge Res. Center, Dec. 1956.

8. Friedrich, Hans R., and Dore, Frank J.: The Dynamic Motion of a Missile Descending Through the Atmosphere. Jour. Aero. Sci., vol. 22, no. 9, Sept. 1955, pp. 628-632, 638.

TABLE I.- INERTIA, WEIGHT, DIMENSIONS, AND STABILITY

DERIVATIVES OF SATELLITE VEHICLE

Parameters:	
I_X, slug-ft^2	1060.39
I_Y, slug-ft^2	4241.57
I_Z, slug-ft^2	4846.78
b, ft	15.0
$\bar{c}$, ft	15.0
W, lb	4060.0
S, sq ft	203.0
W/S, lb/sq ft	20.0
Standard stability derivatives (The first term in the damping and control effectiveness derivatives that follow is the aerodynamic contribution and the second term is the reaction jet contribution.):	
C_{l_ϕ}, 1/radian	-0.13
C_{m_α}, 1/radian	-0.13
C_{n_ψ}, 1/radian	0
C_{l_p}, 1/radian/sec	$-0.344\left(0.0680 + \frac{0.0226}{\bar{q}}\right)$
C_{m_q}, 1/radian/sec	$-0.458\left(0.0680 + \frac{0.0405}{\bar{q}}\right)$
C_{n_r}, 1/radian/sec	$-1.146\left(0.0174 + \frac{0.0461}{\bar{q}}\right)$
$C_{l_{\delta_1}}$, 1/radian	$0.0680 + \frac{0.0226}{\bar{q}}$
$C_{m_{\delta_2}}$, 1/radian	$0.0680 + \frac{0.0405}{\bar{q}}$
$C_{n_{\delta_3}}$, 1/radian	$0.0174 + \frac{0.0461}{\bar{q}}$
Force coefficients:	
C_N	1.7
C_c	0
Standard cross-control moment derivatives:	
$C_{l_{\delta_2}}$, 1/radian	0
$C_{l_{\delta_3}}$, 1/radian	$-1.0C_{n_{\delta_3}}$
$C_{m_{\delta_1}}$, 1/radian	$-0.5C_{l_{\delta_1}}$
$C_{m_{\delta_3}}$, 1/radian	$-0.5C_{n_{\delta_3}}$
$C_{n_{\delta_1}}$, 1/radian	$-1.0C_{l_{\delta_1}}$
$C_{n_{\delta_2}}$, 1/radian	0

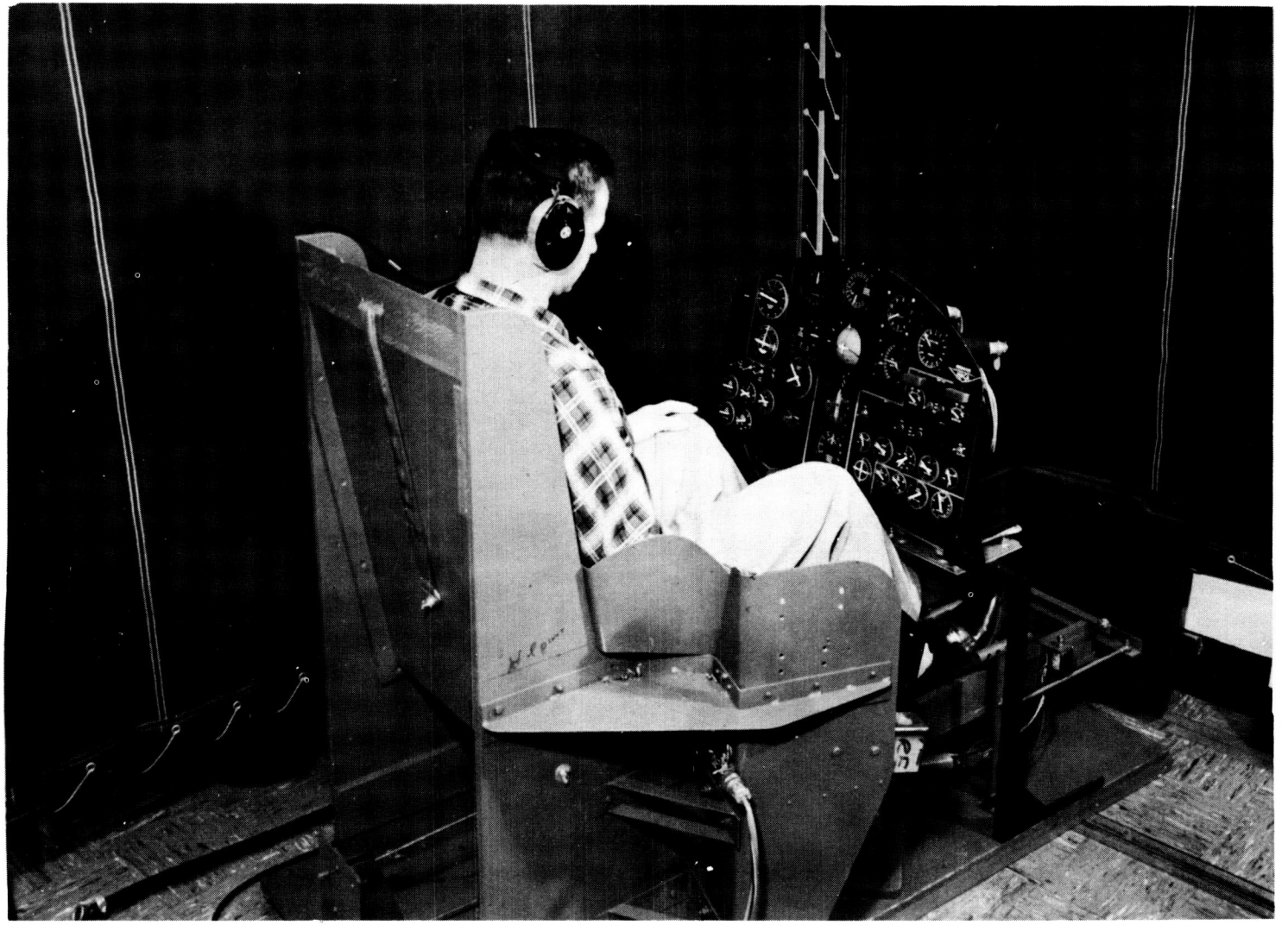

Figure 1.- Fixed-base simulator. L-59-237

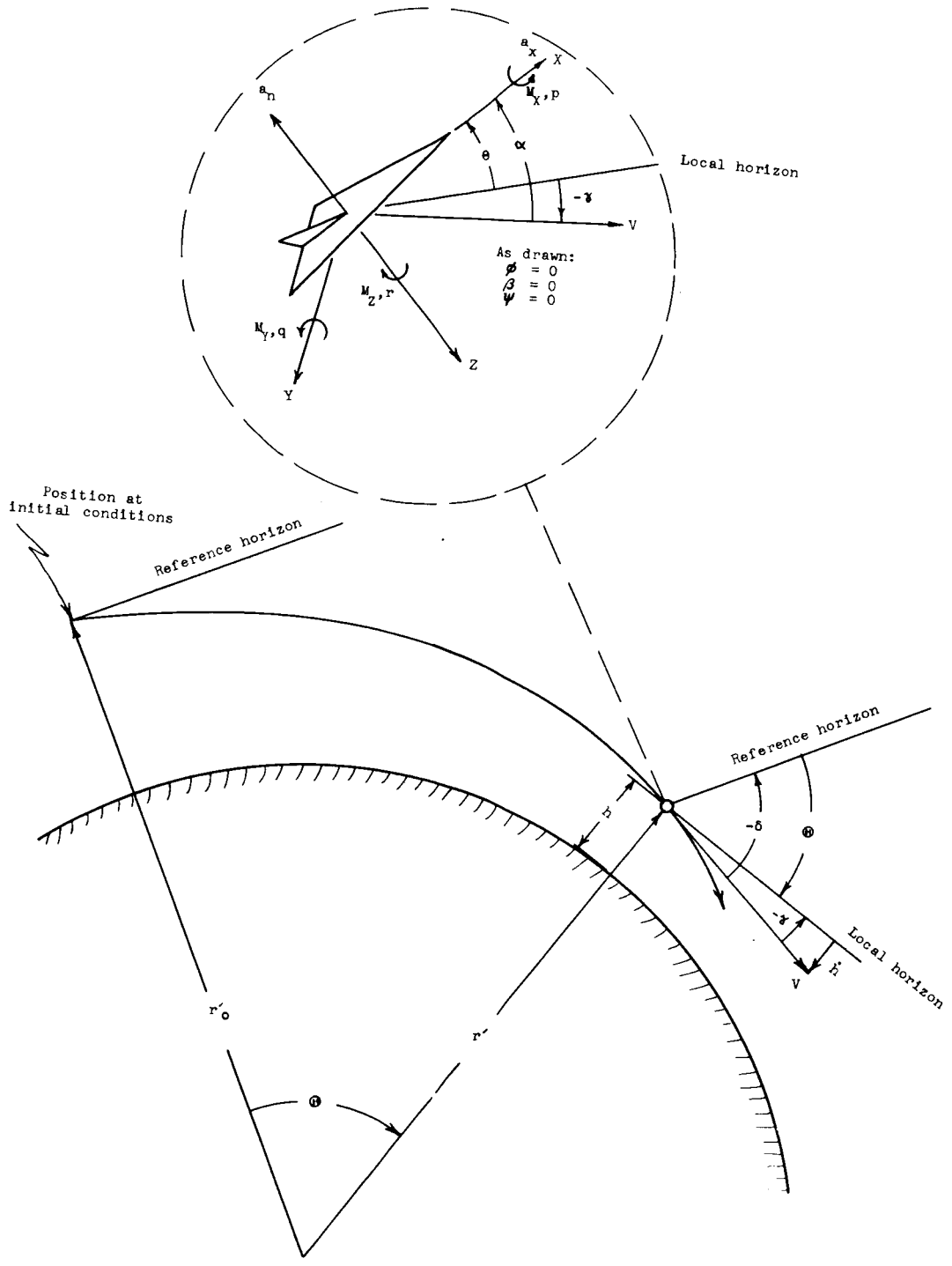

Figure 2.- Sign convention and symbols used to describe the motion of vehicle entering the earth's atmosphere.

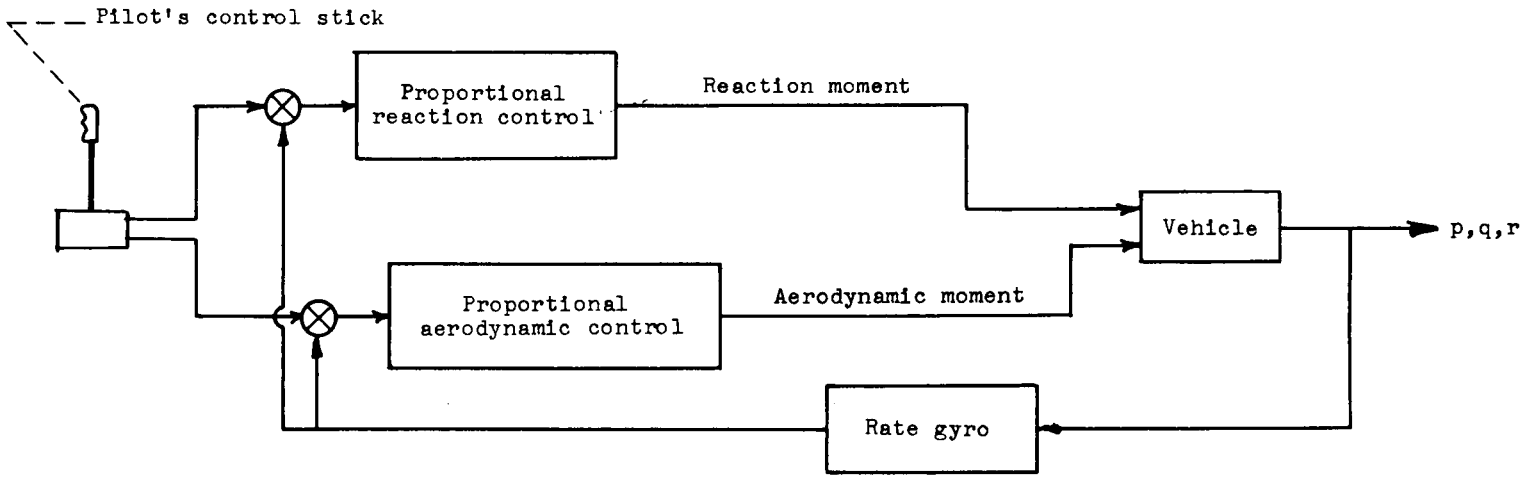

Figure 3.- Schematic block diagram showing relationship between pilot's controls, damping, and vehicle control moments.

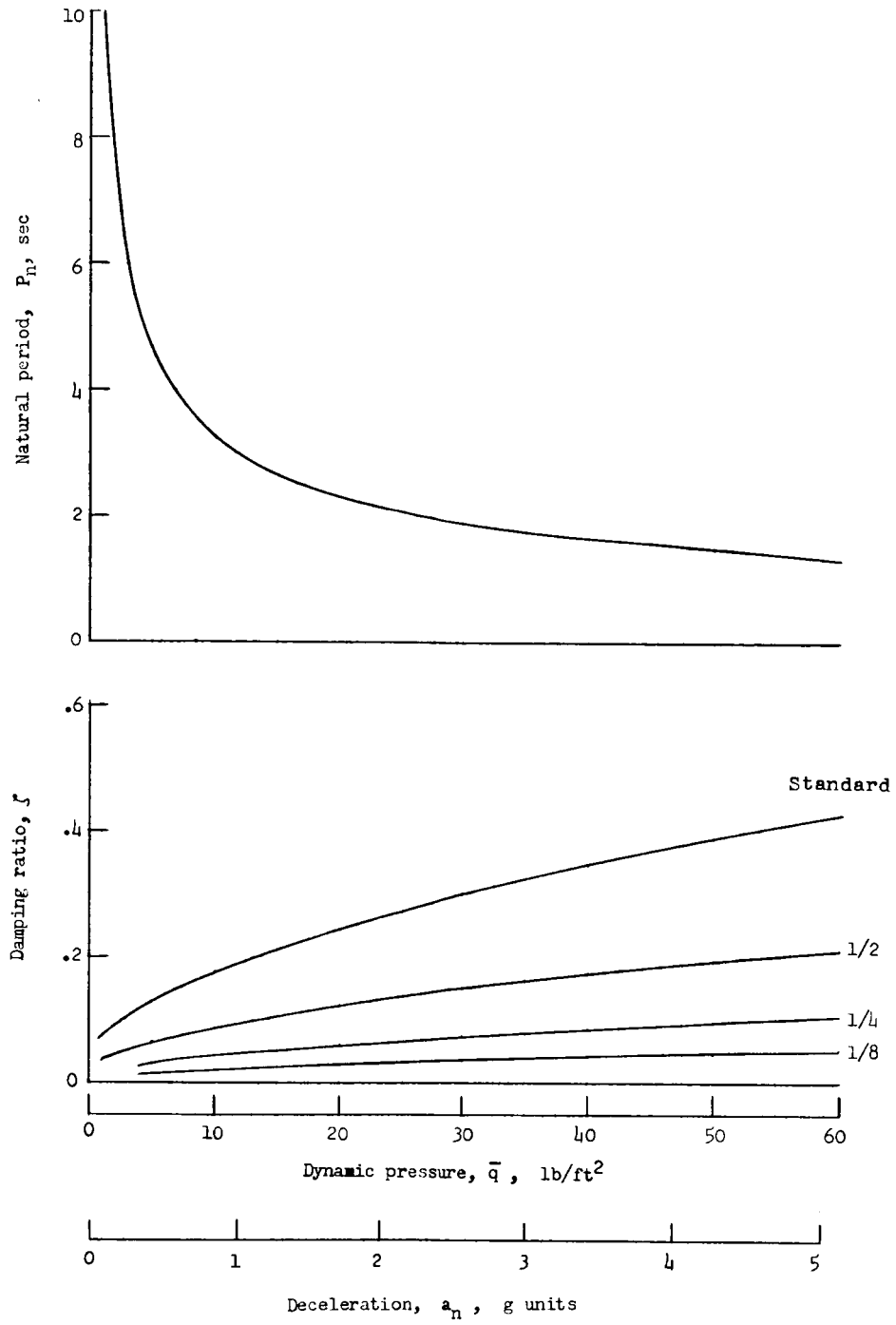

(a) Roll damping and period.

Figure 4.- Variation of stability with dynamic pressure.

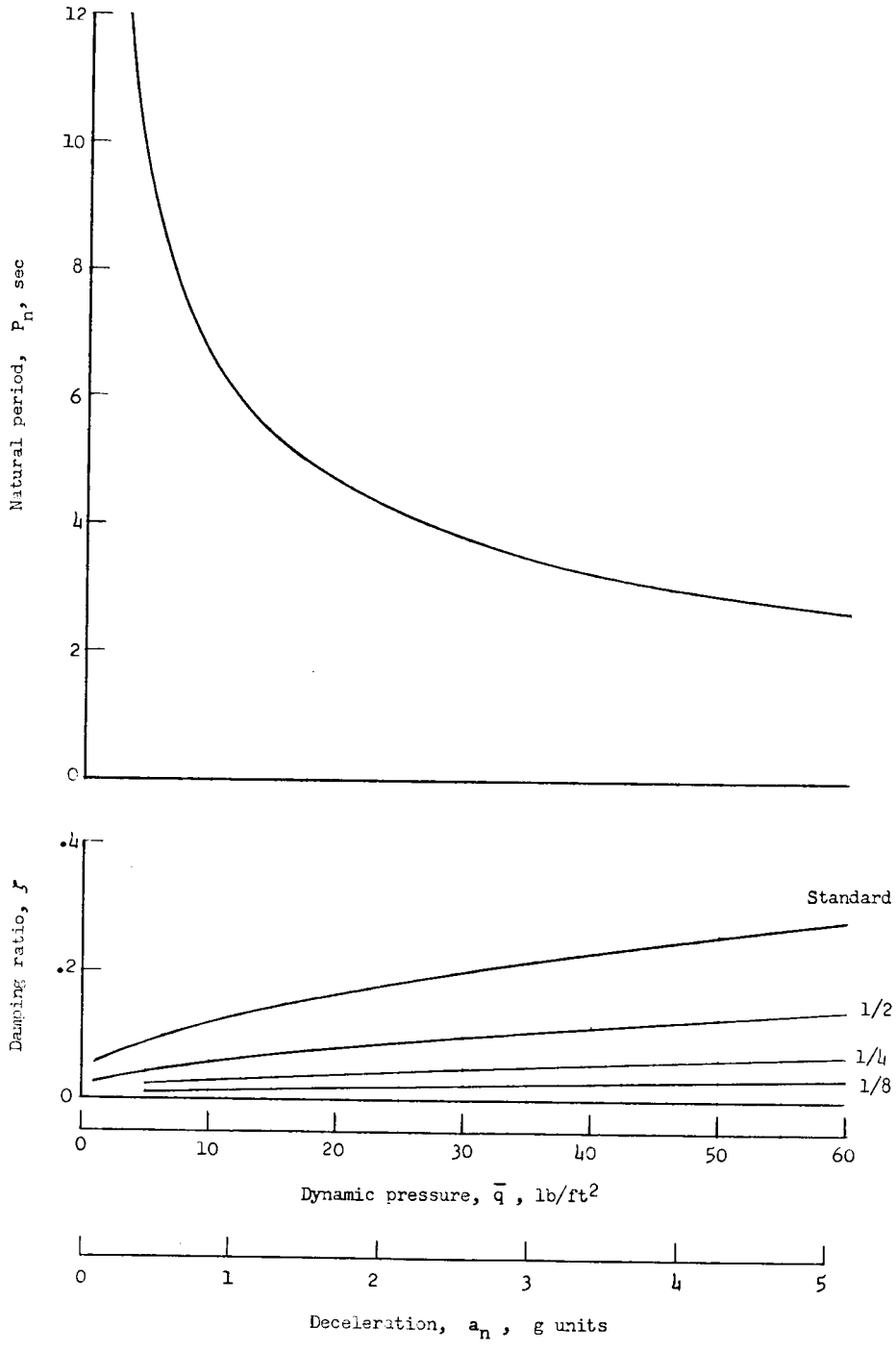

(b) Pitch damping and period.

Figure 4.- Continued.

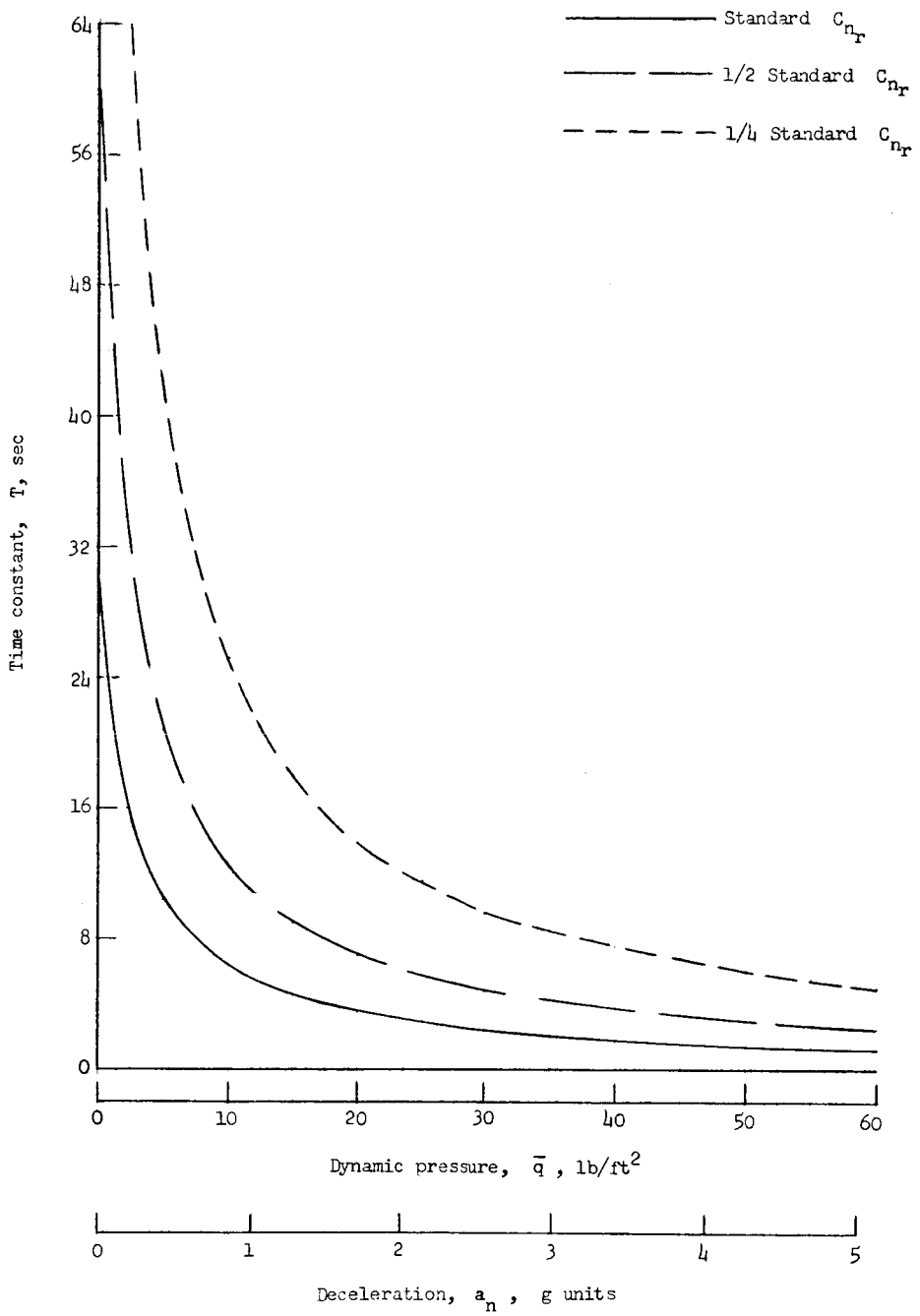

(c) Yaw time constant.

Figure 4.- Concluded.

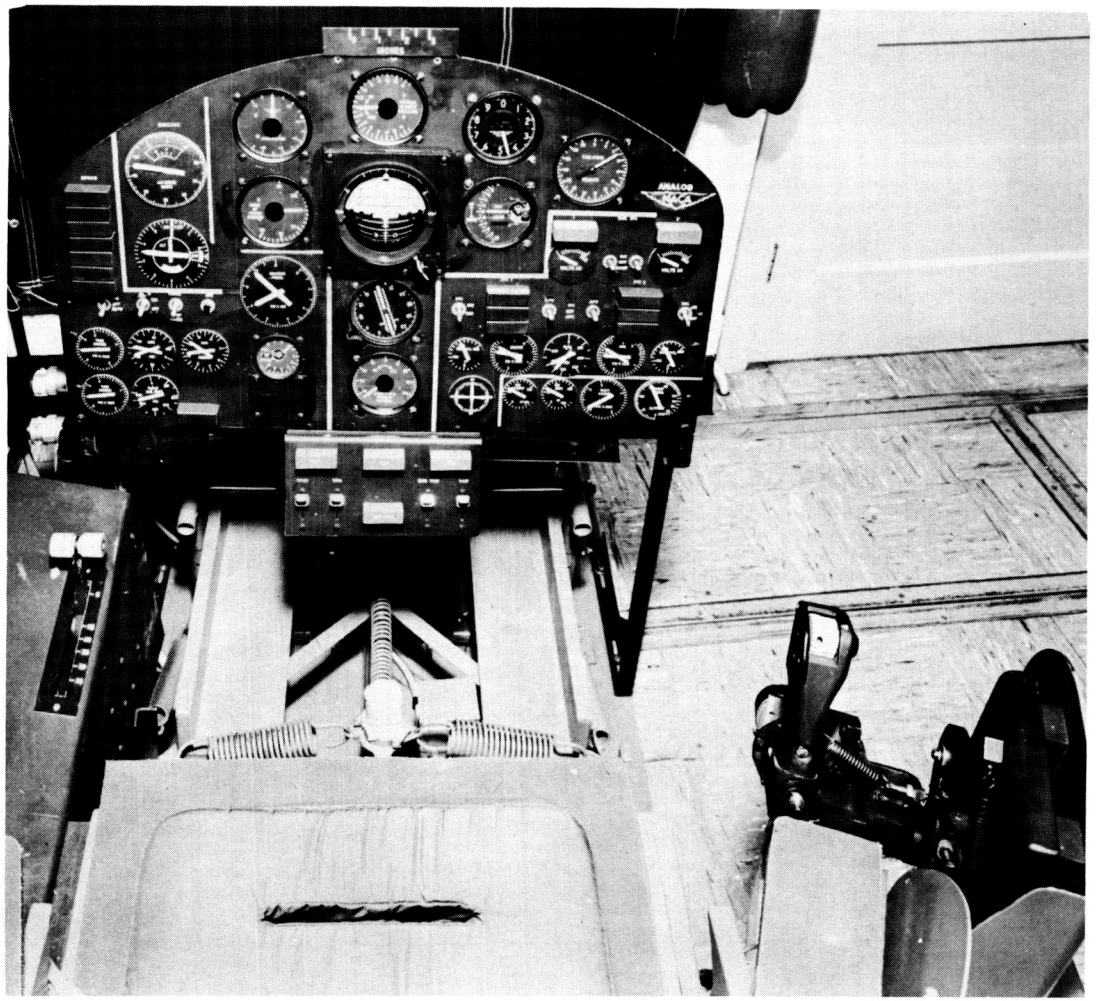

(a) General layout of cockpit. L-58-1129a

Figure 5.- Simulator cockpit layout showing side-arm controllers and instrument panel.

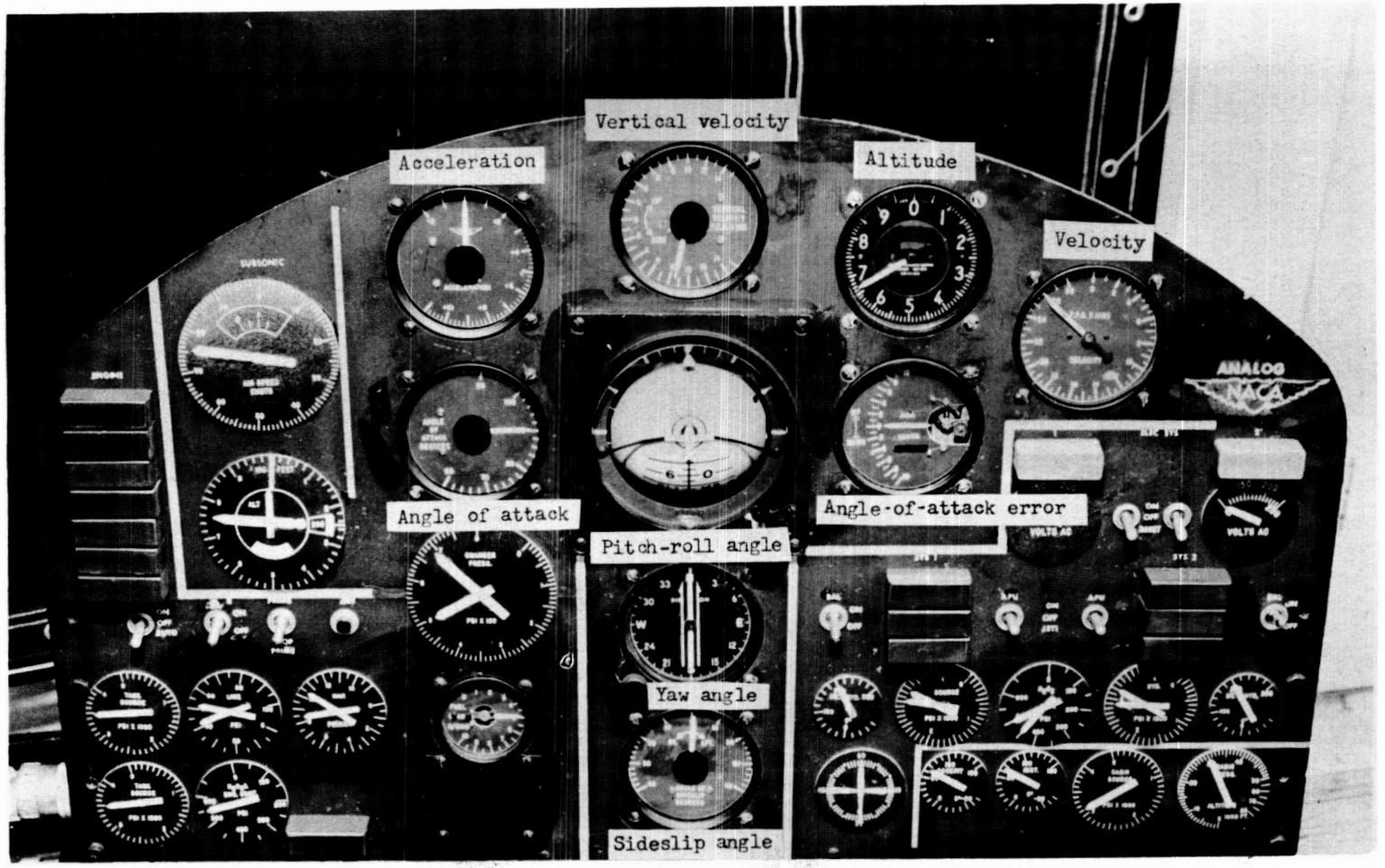

(b) Instrument panel detail. L-59-234.1

Figure 5.- Continued.

L-808

(c) Grip-type side-arm controller. Side view. L-59-4228

Figure 5.- Continued.

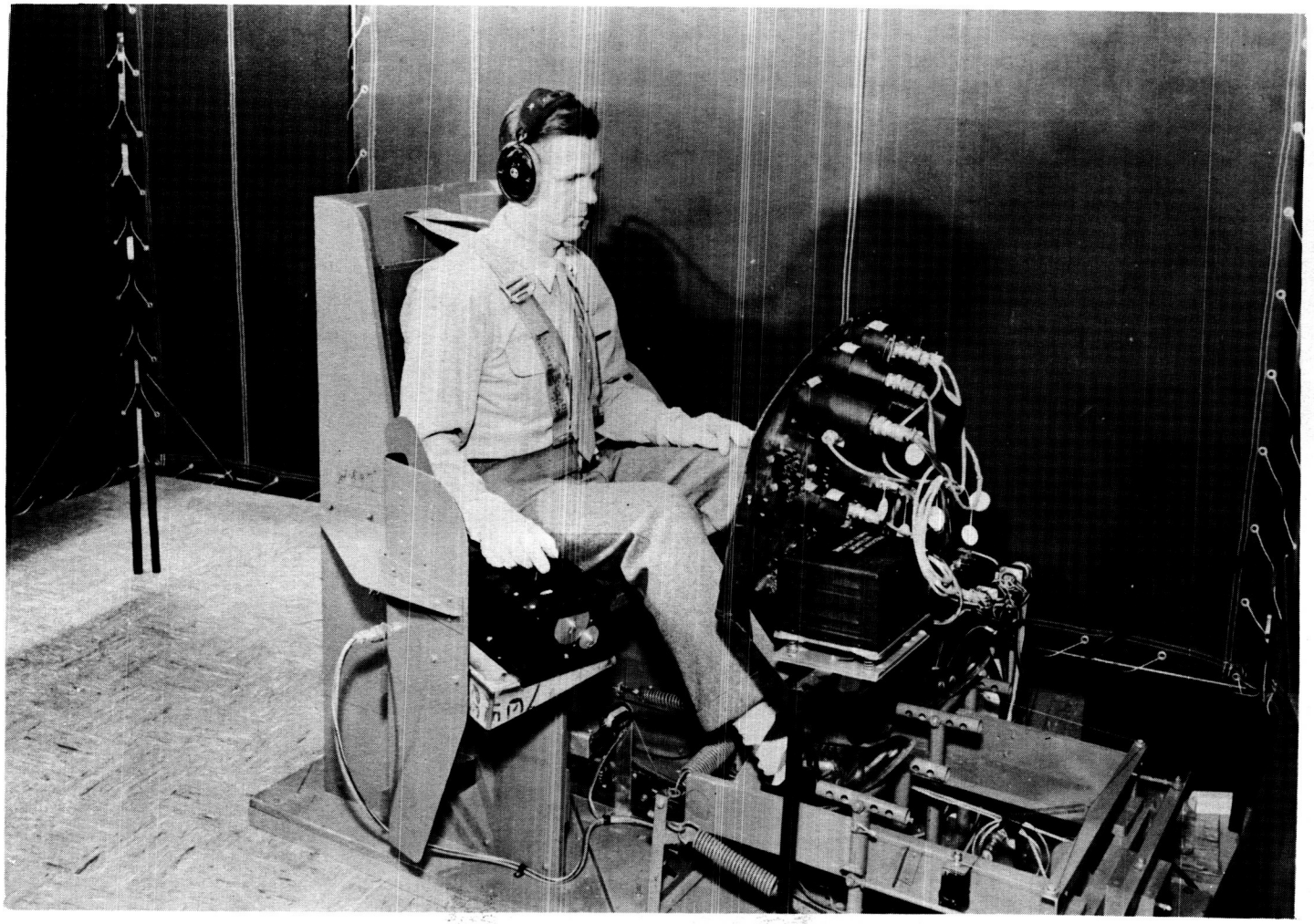

(d) Finger-tip side-arm controller. Front view. L-59-238

Figure 5.- Concluded.

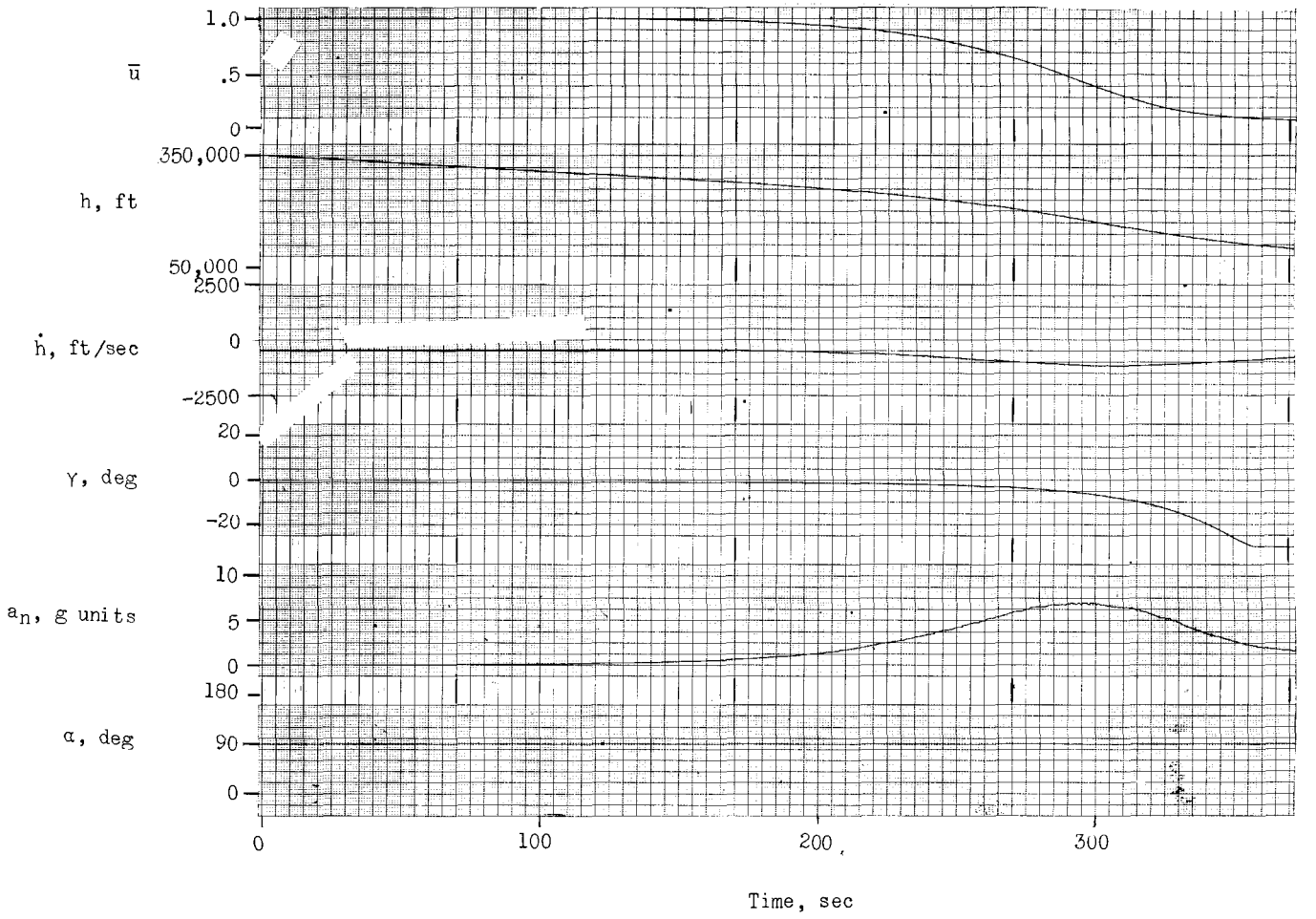

(a) $\gamma_o = -1^o$; $\alpha = 90^o$.

Figure 6.- Time histories of body with W/S = 20 during atmospheric entry. V_o = 25,863 ft/sec; h_o = 350,000 ft.

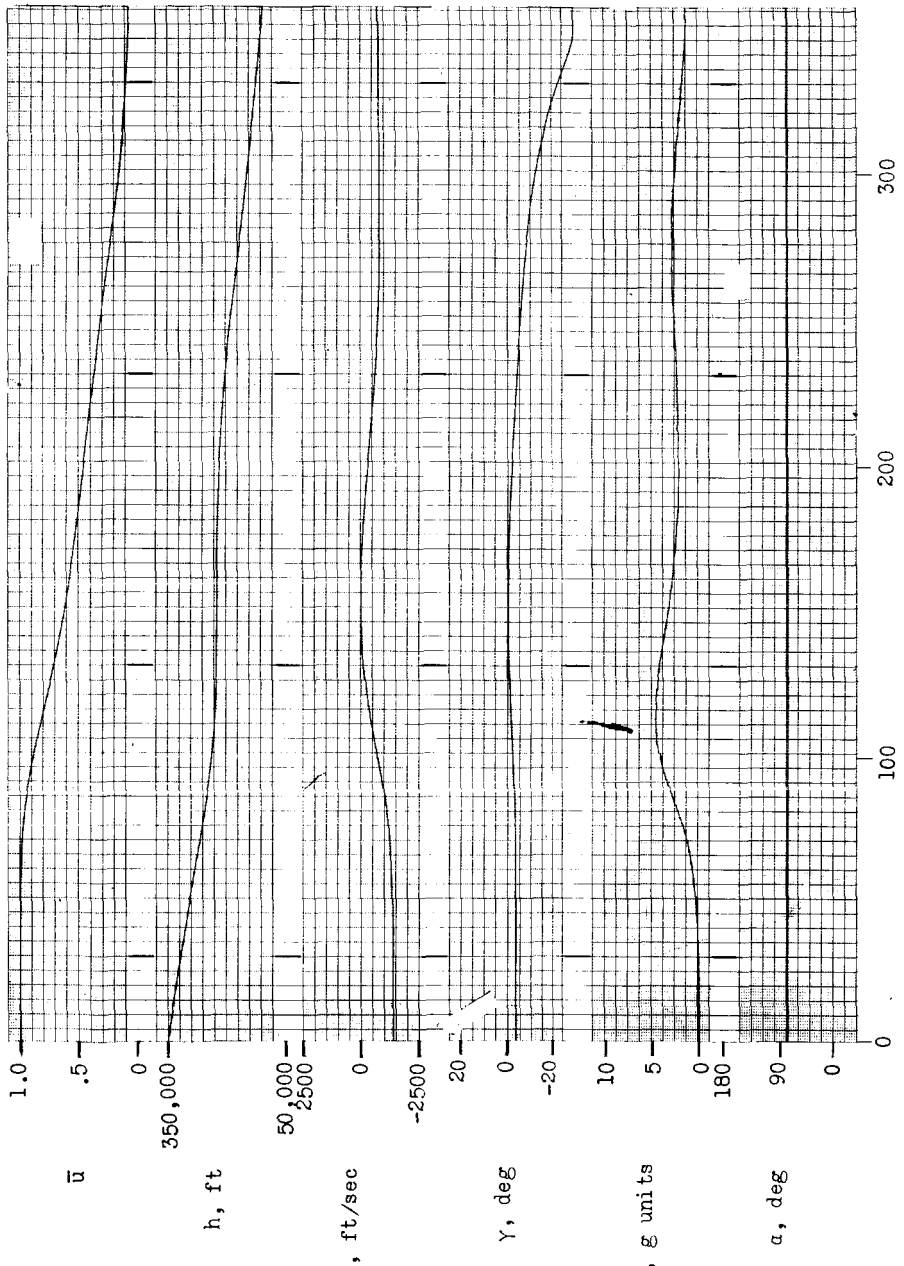

(b) $\gamma_o = -3^o$; $\alpha = 79^o$.

Figure 6.- Concluded.

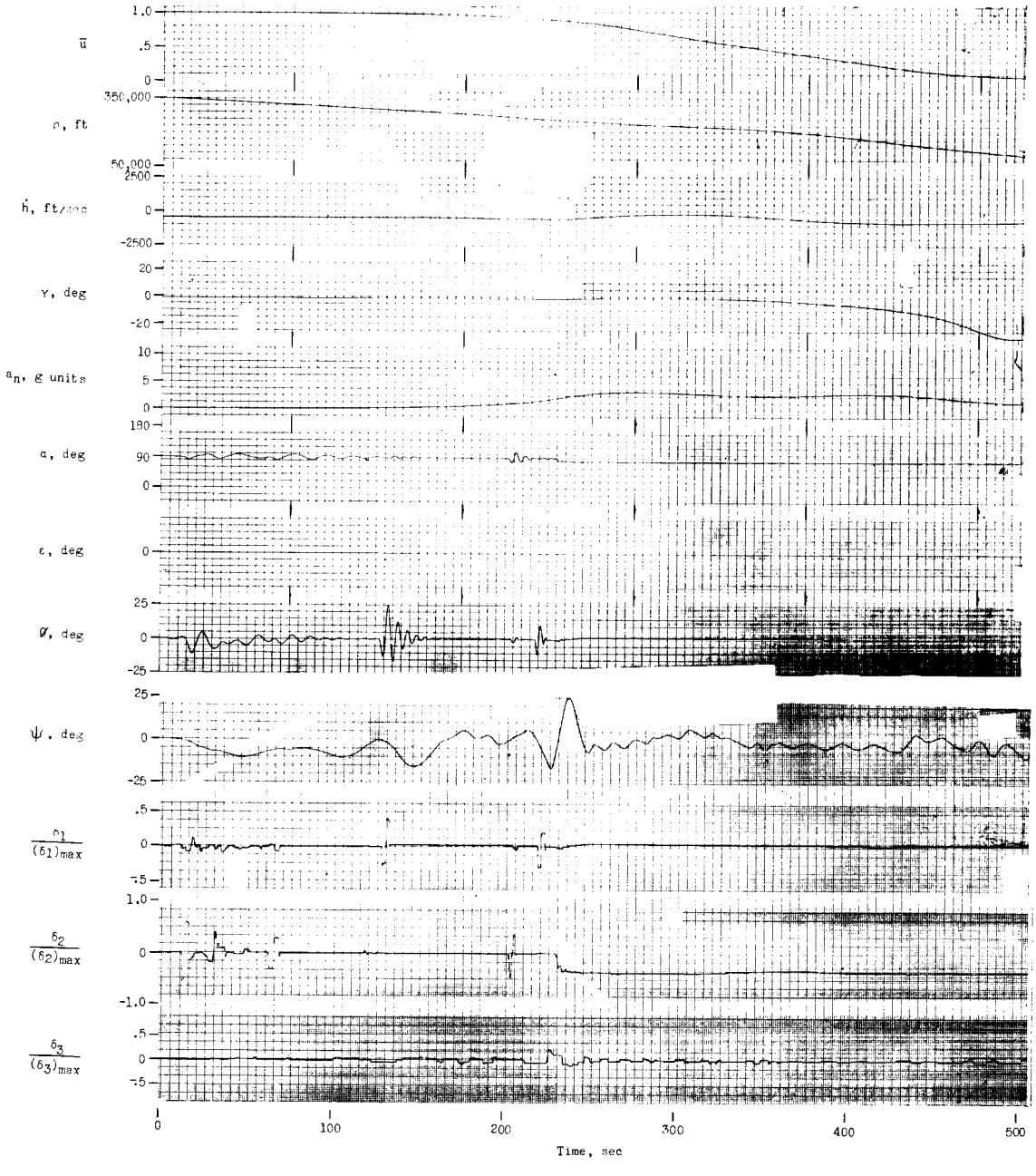

(a) Step reduction in angle of attack at 2g. $\gamma_o = -1^o$.

Figure 7.- Simulated entries for three types of pilot control tasks. V_o = 25,863 ft/sec; h_o = 350,000 ft; $\alpha_o = 90^o$.

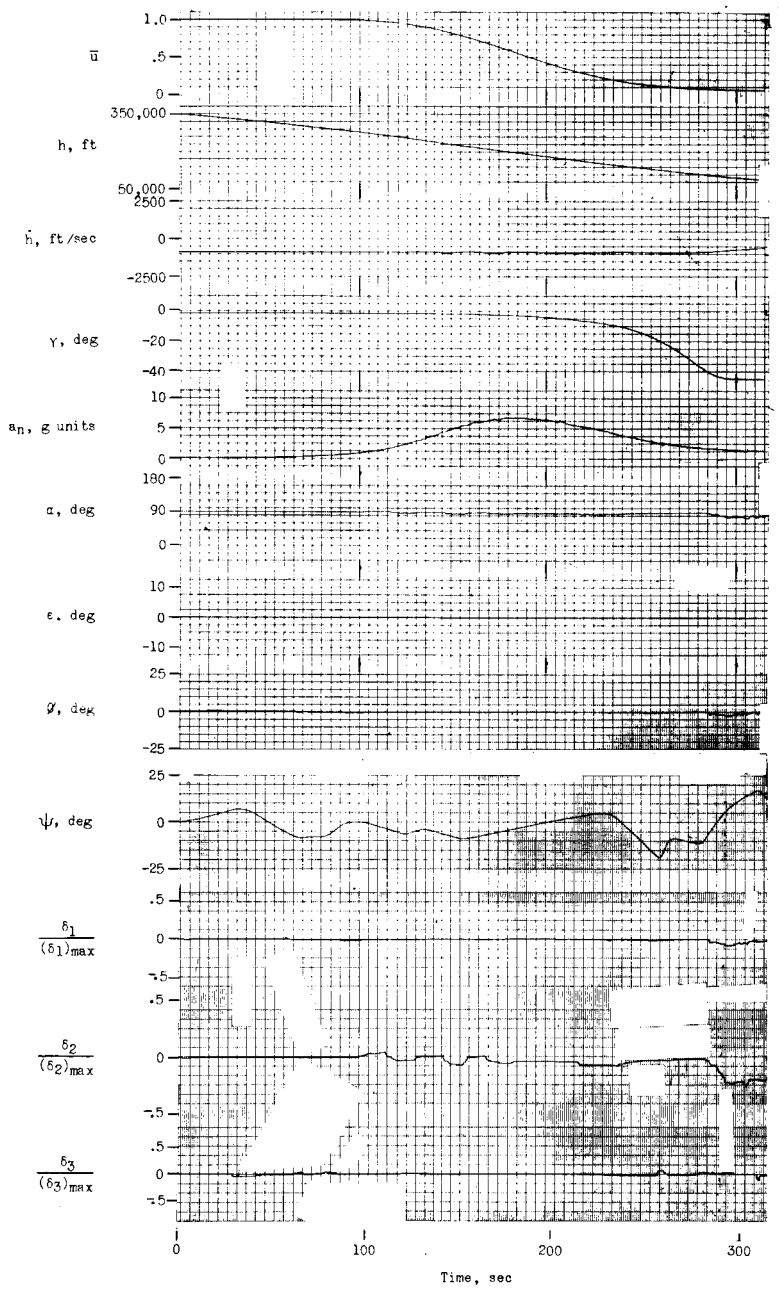

(b) Constant rate of descent. $\gamma_o = -2^o$.

Figure 7.- Continued.

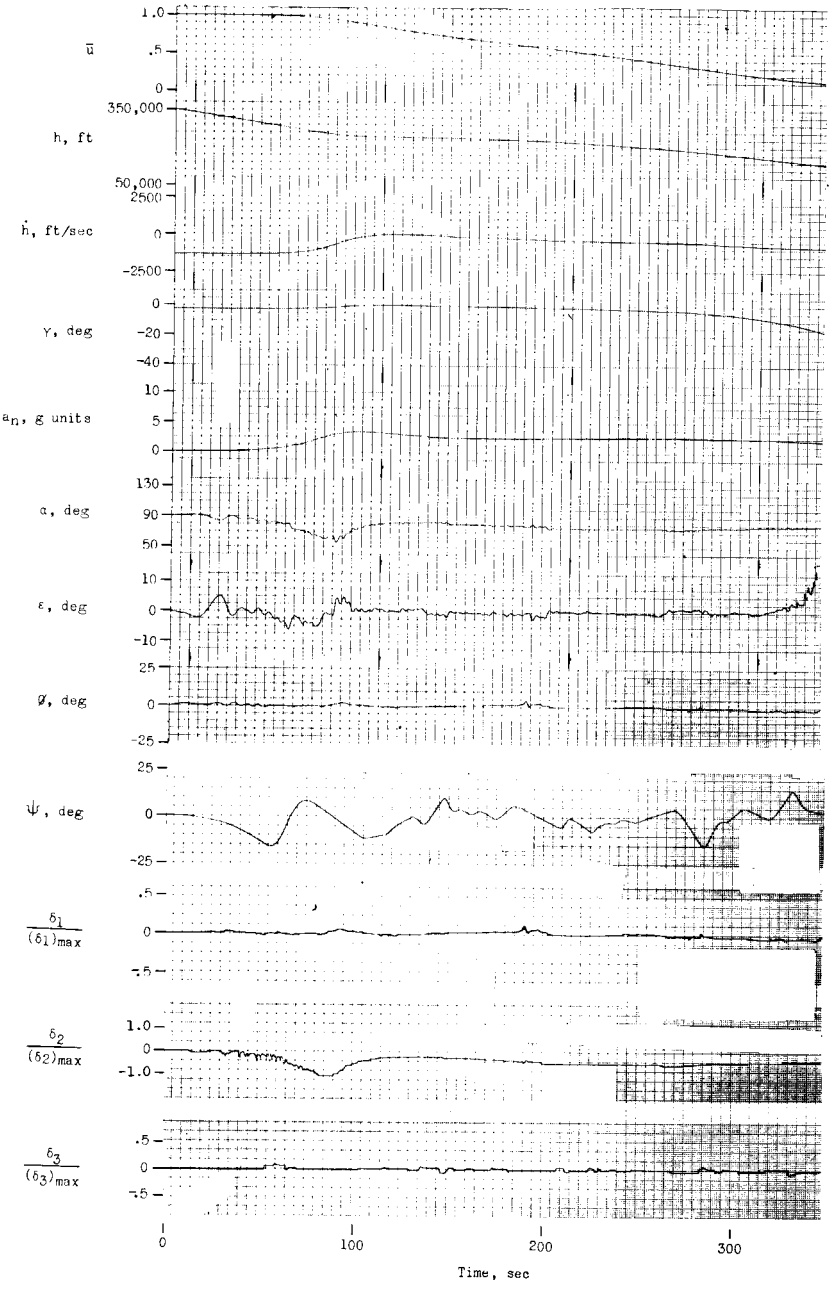

(c) Maintenance of zero angle-of-attack error. $\gamma_o = -3^o$.

Figure 7.- Concluded.

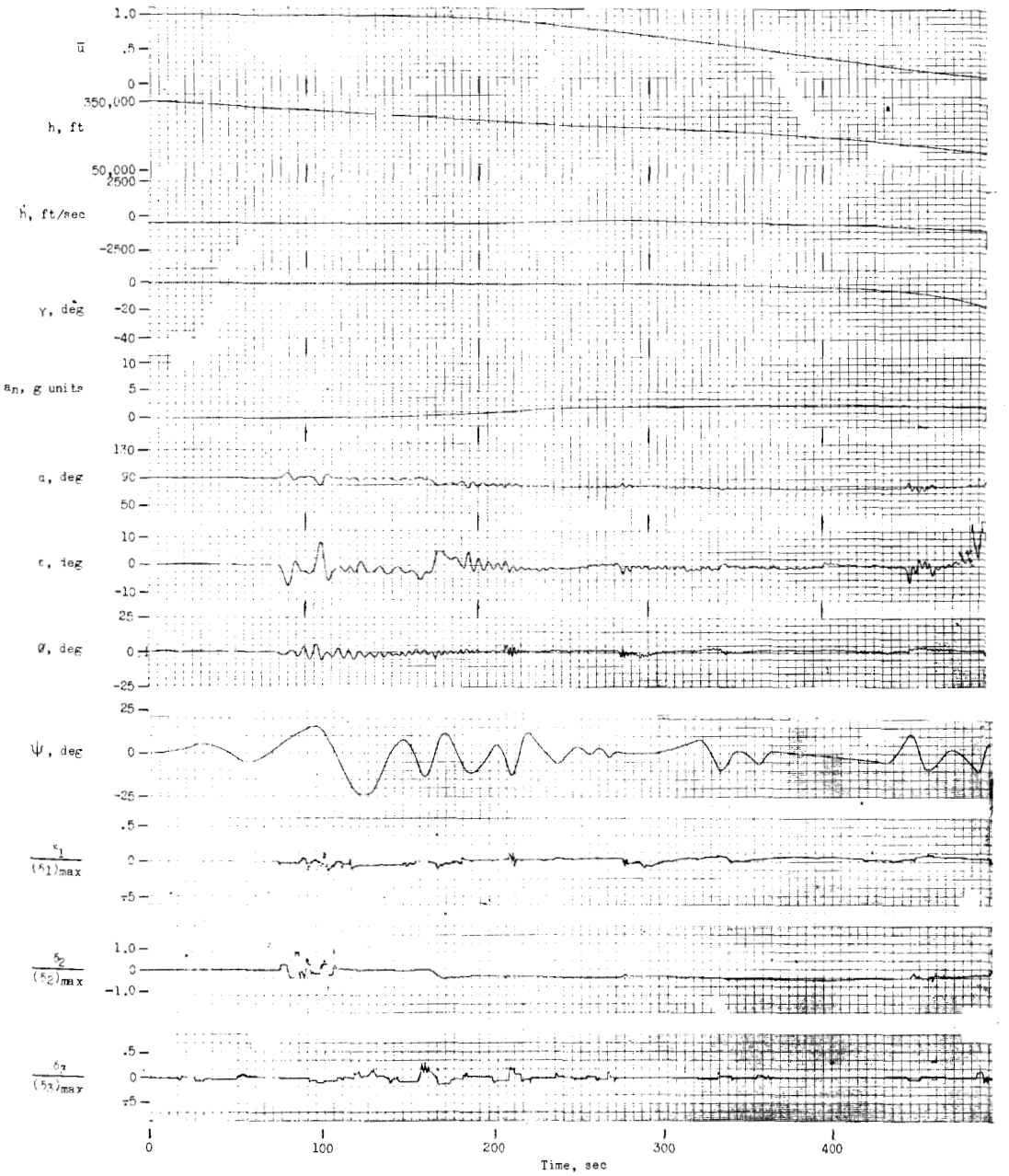

(a) 1/2 standard damping.

Figure 8.- Variation in damping during simulated entries. Piloting task was to maintain zero angle-of-attack error. V_o = 25,863 ft/sec; h_o = 350,000 ft; γ_o = -1°; α_o = 90°.

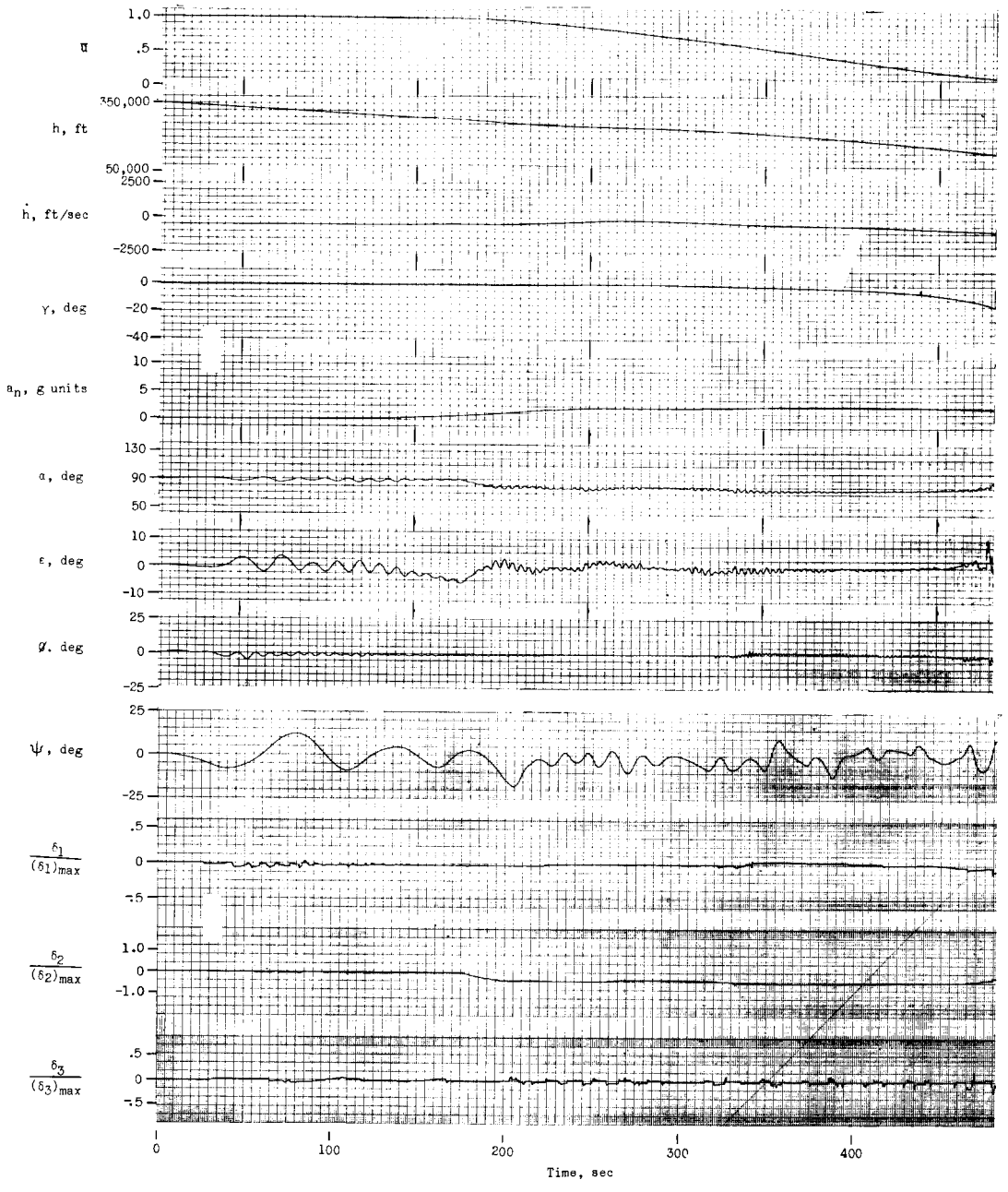

(b) 1/4 standard damping.

Figure 8.- Continued.

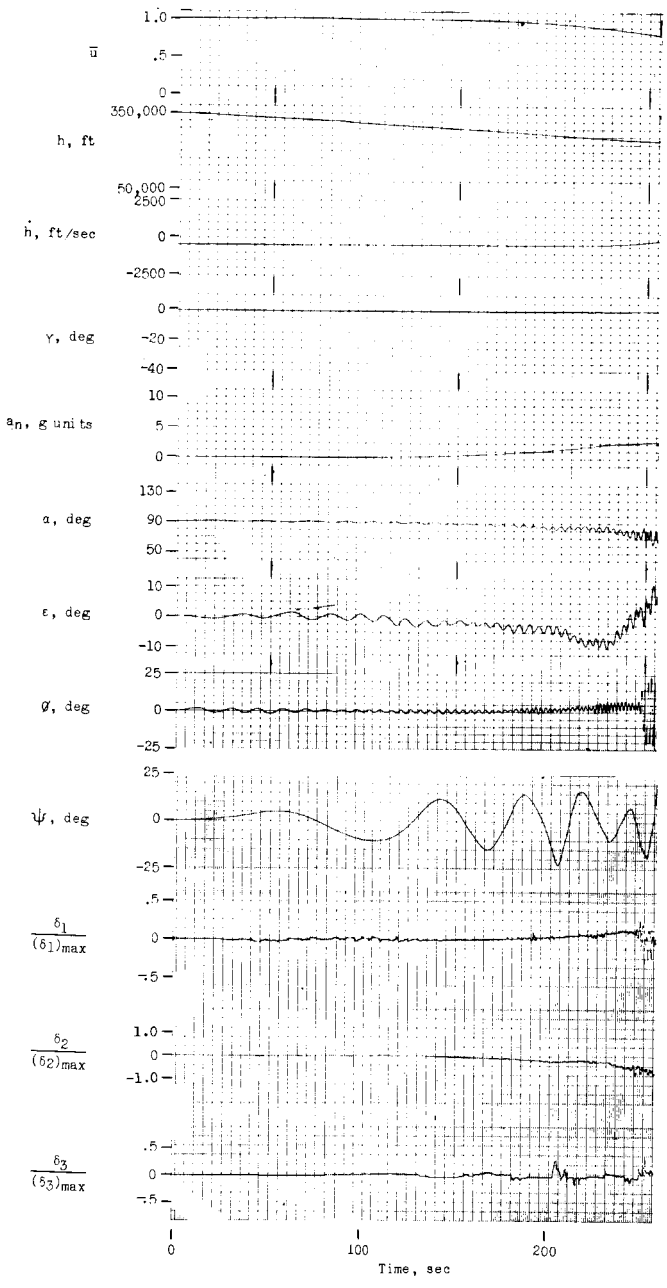

(c) 1/8 standard damping.

Figure 8.- Continued.

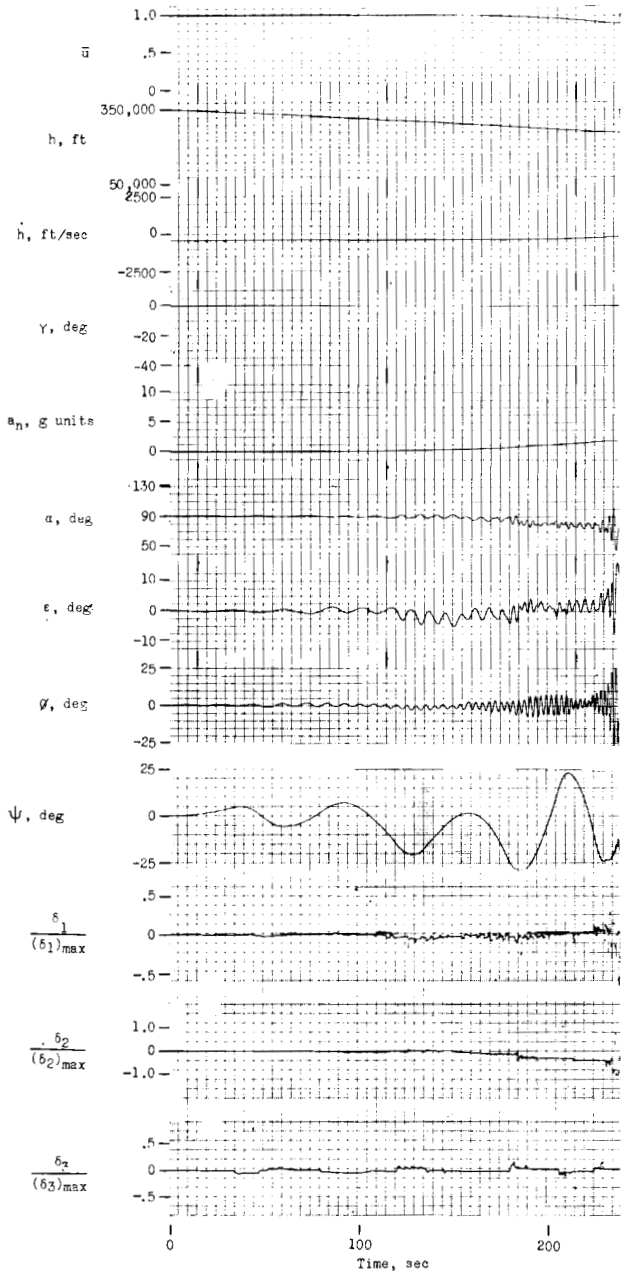

(d) Zero standard damping.

Figure 8.- Continued.

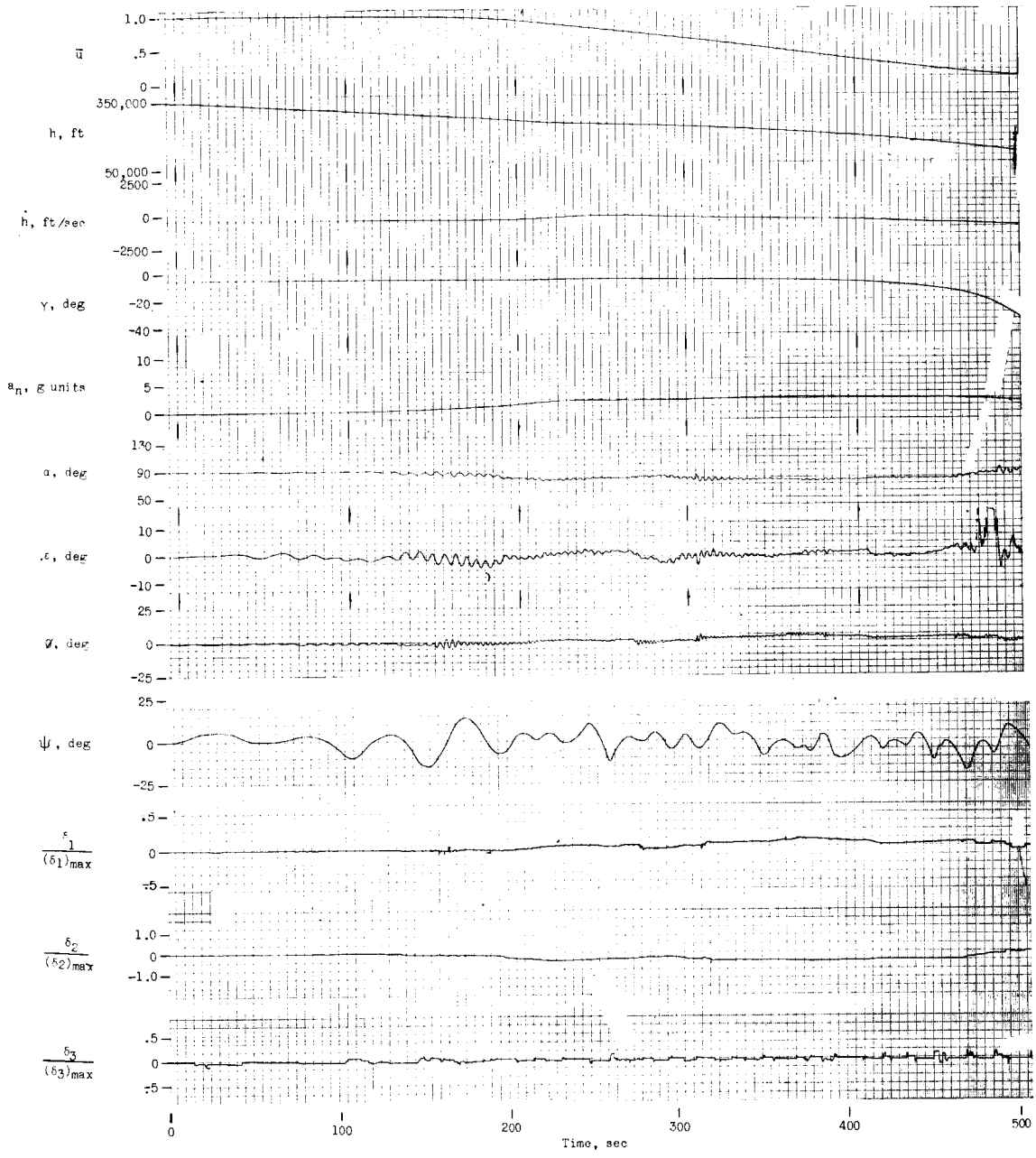

(e) 1/4 standard aerodynamic damping; zero reaction control damping.

Figure 8.- Concluded.

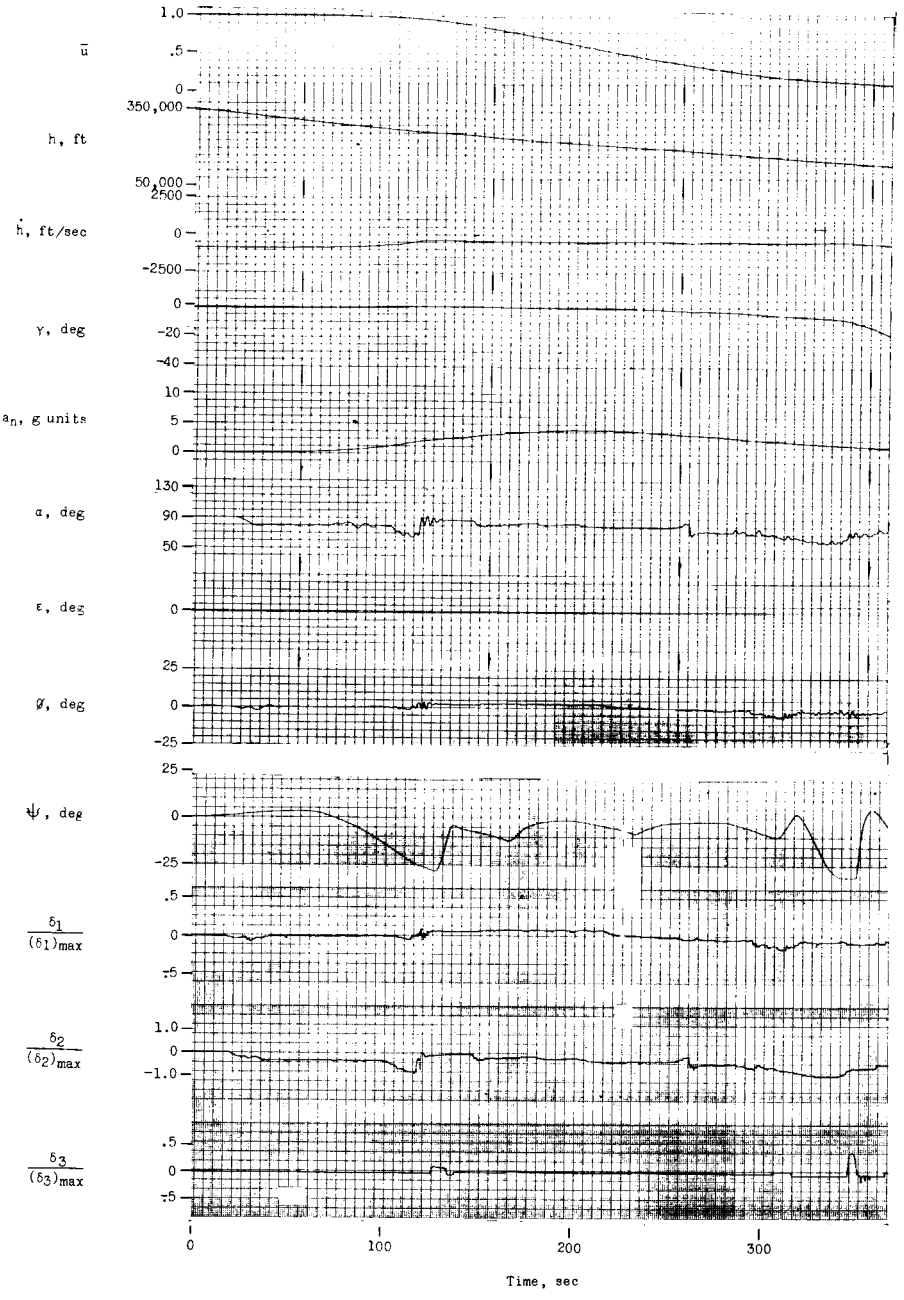

(a) 1/2 standard effectiveness.

Figure 9.- Variation in reaction control effectiveness. Piloting task was to reduce rate of descent to 450 feet per second. V_o = 25,863 ft/sec; h_o = 350,000 ft; γ_o = -2°; α_o = 90°.

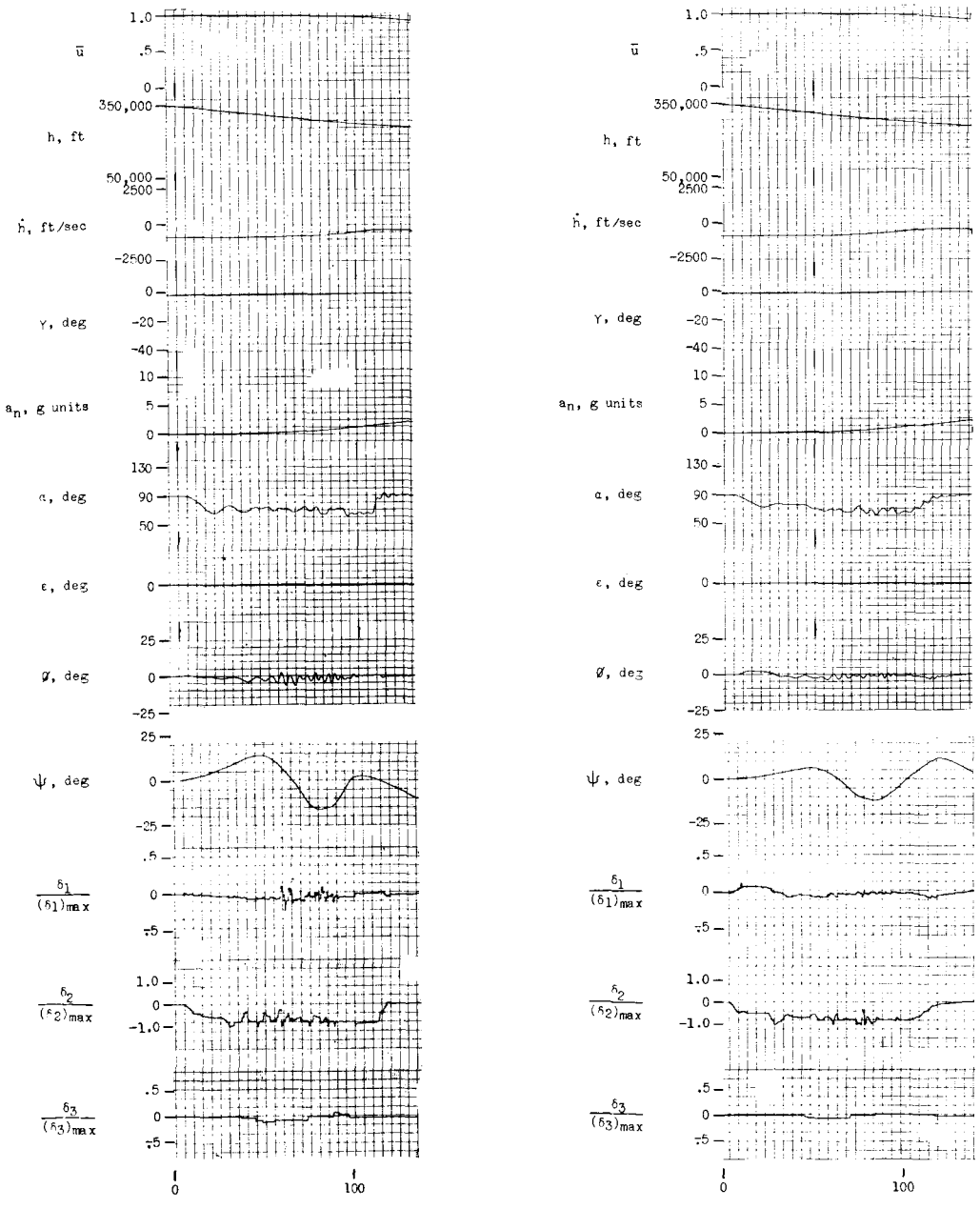

(b) 1/4 standard effectiveness. (c) 1/8 standard effectiveness.

Figure 9.- Concluded.

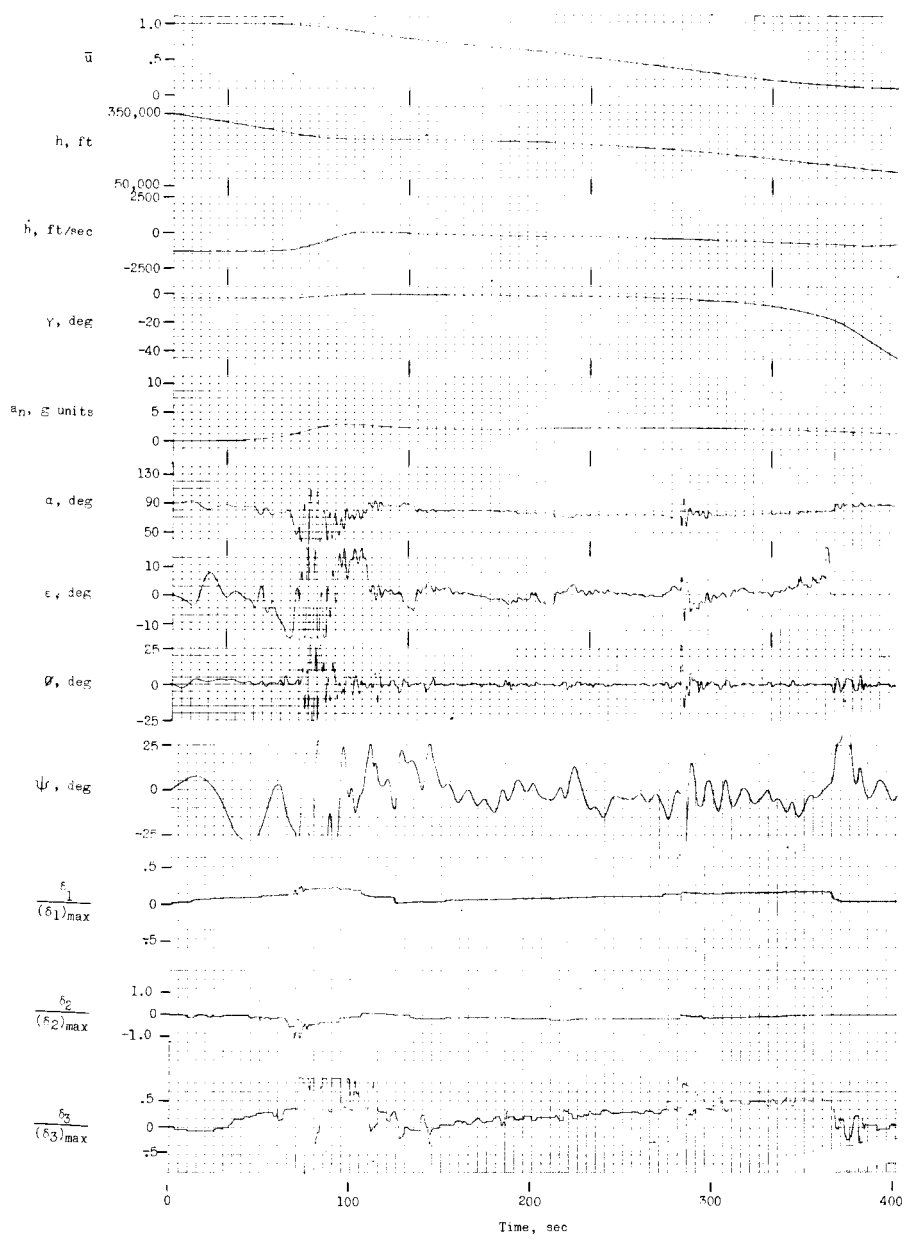

(a) Standard damping; standard coupling; control pulses.

Figure 10.- Variation in adverse aerodynamic-control moment coupling. Piloting task was to maintain zero angle-of-attack error. V_o = 25,863 ft/sec; h_o = 350,000 ft; γ_o = -3°; α_o = 90°.

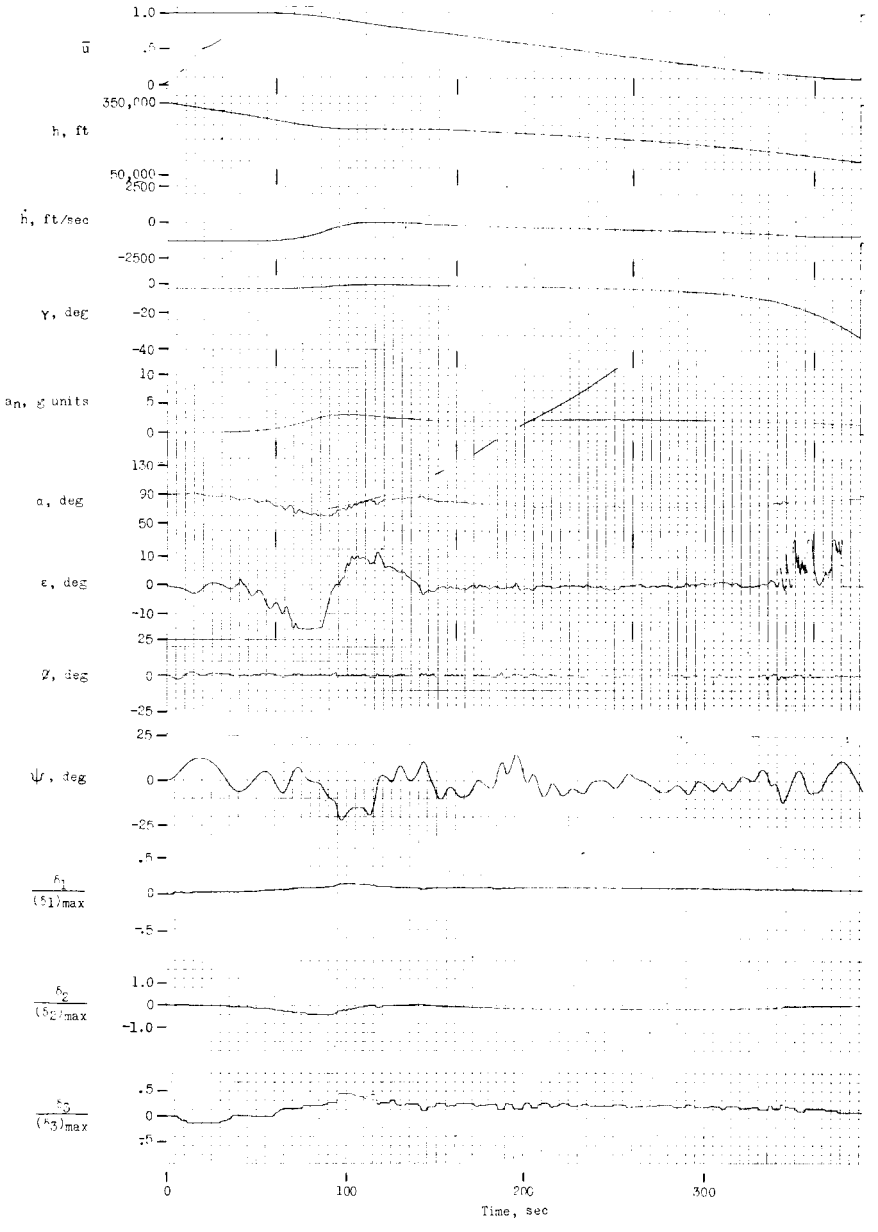

(b) Standard damping; standard coupling; no control pulses.

Figure 10.- Continued.

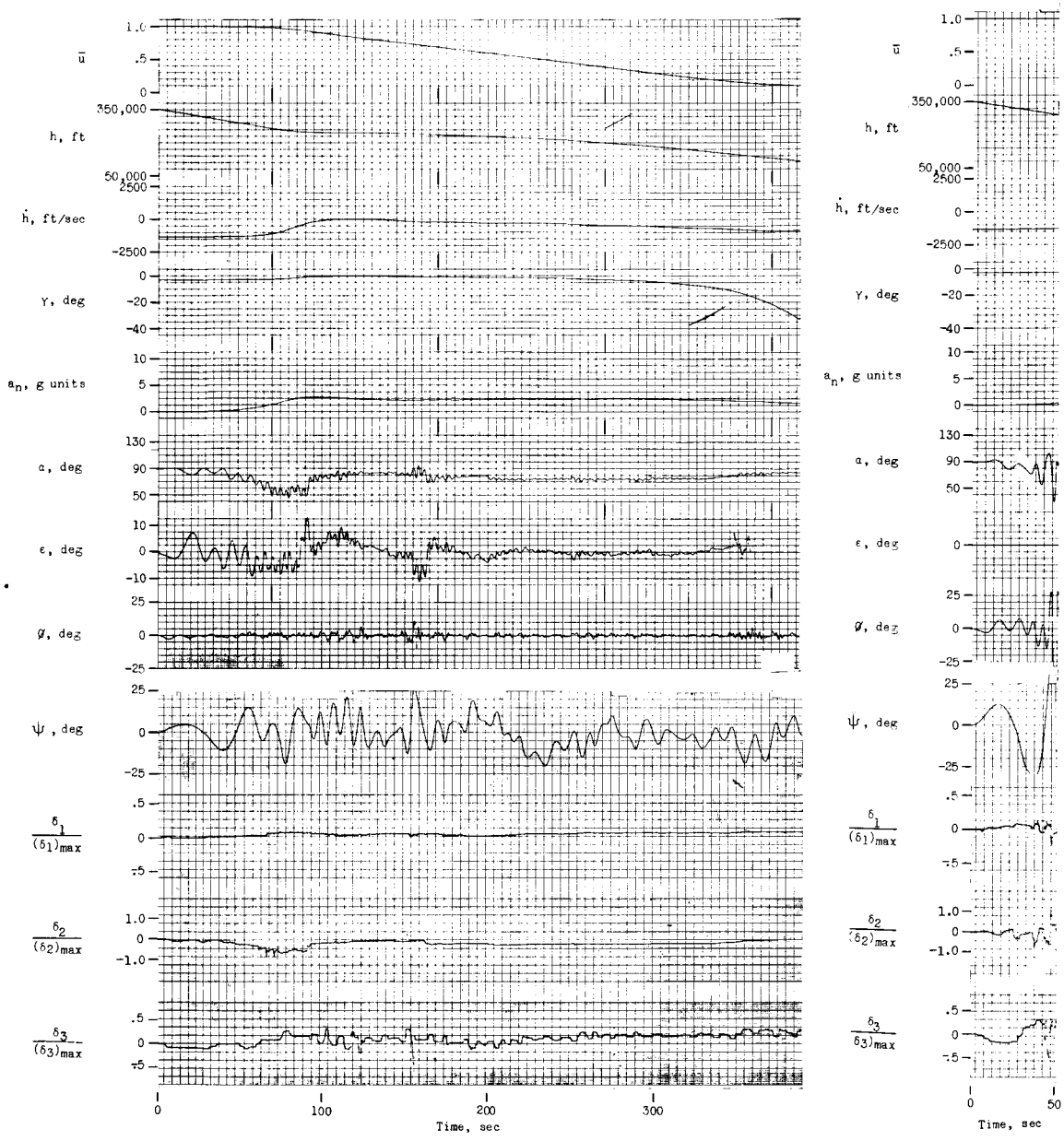

(c) 1/2 standard damping; standard coupling.

(d) 1/2 standard damping; standard coupling.

Figure 10.- Concluded.

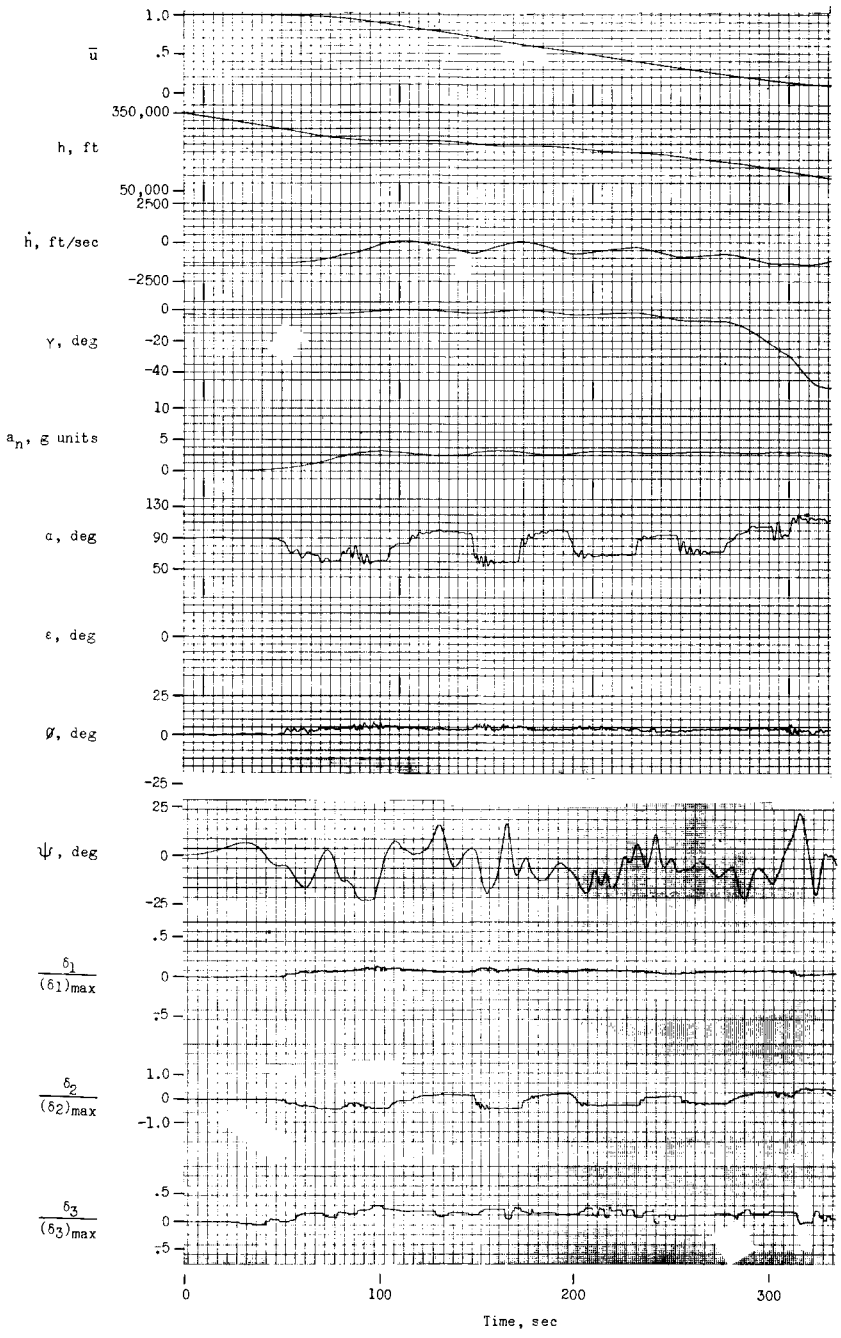

(a) $\gamma_o = -3^o$. Piloting task was to establish and maintain a 3g deceleration.

Figure 11.- Atmospheric entries at flight-path angles up to -6^o. V_o = 25,863 ft/sec; h_o = 350,000 ft; $\alpha_o = 90^o$.

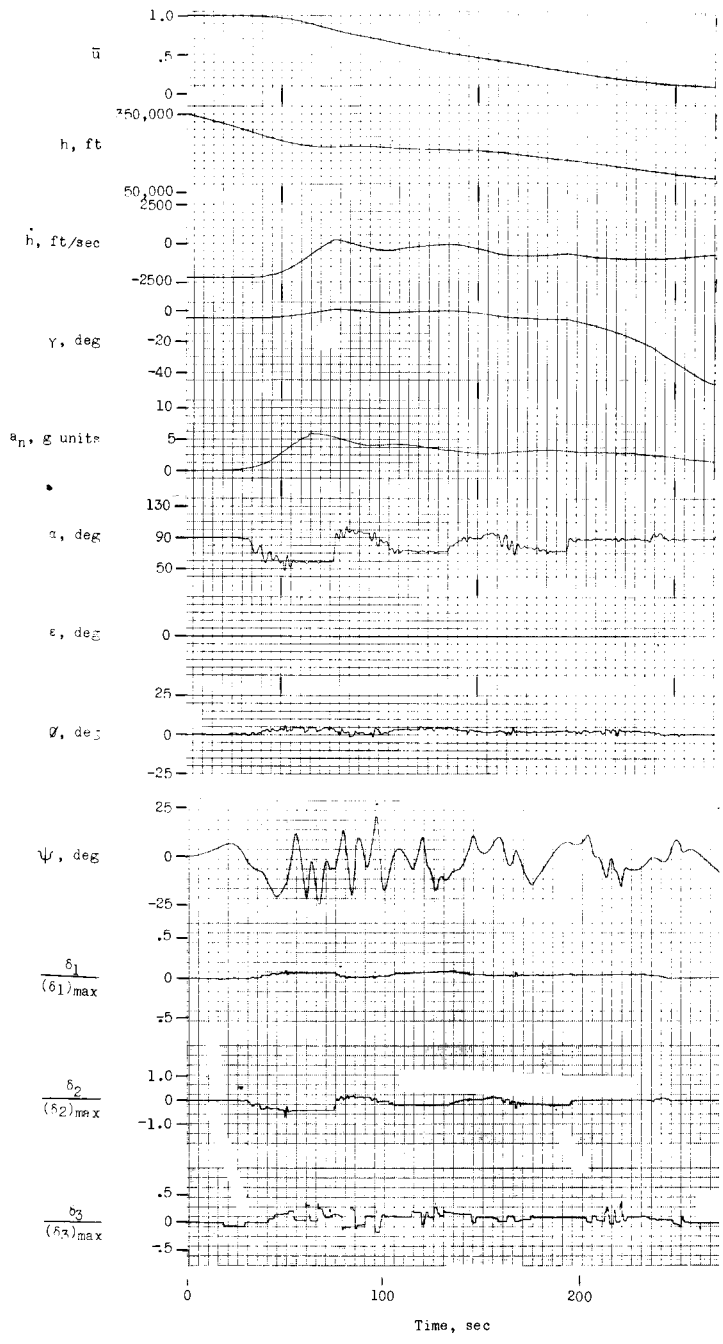

(b) $\gamma_o = -5^o$. Piloting task was to establish and maintain 3g decleration.

Figure 11.- Continued.

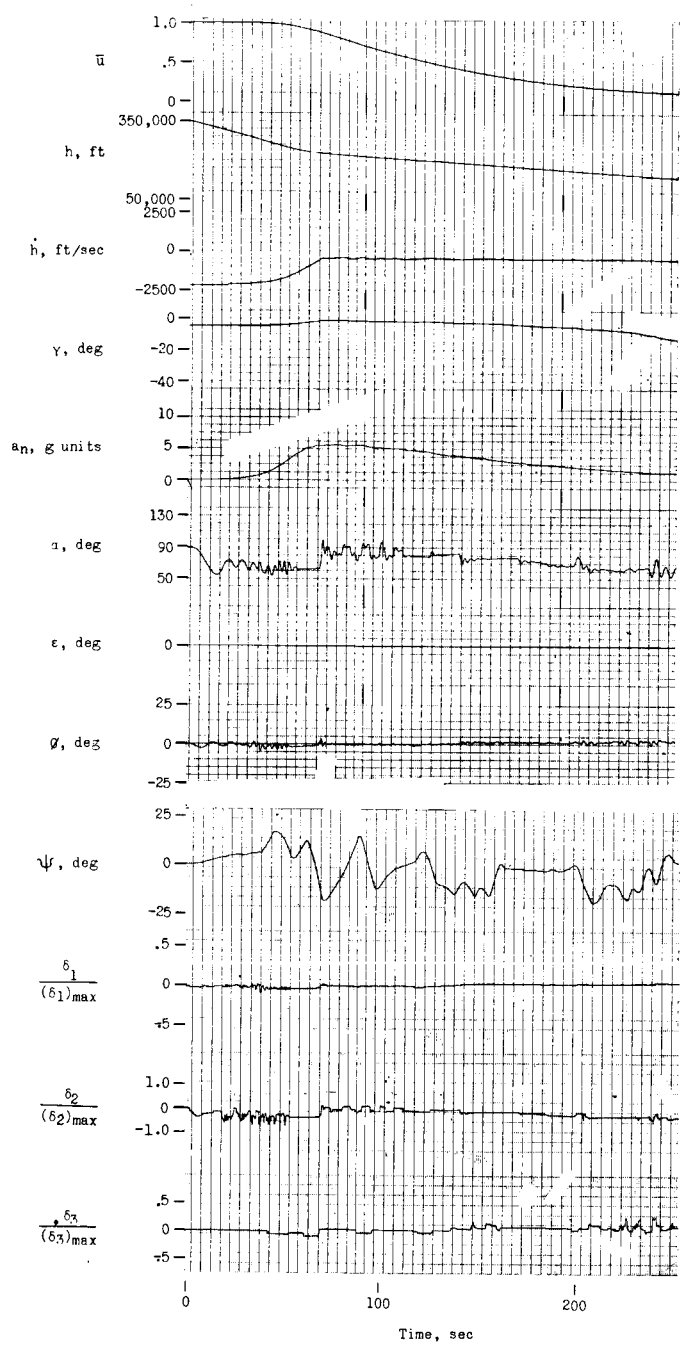

(c) $\gamma_o = -5^o$. Piloting task was to reduce rate of descent to 450 feet per second.

Figure 11.- Continued.

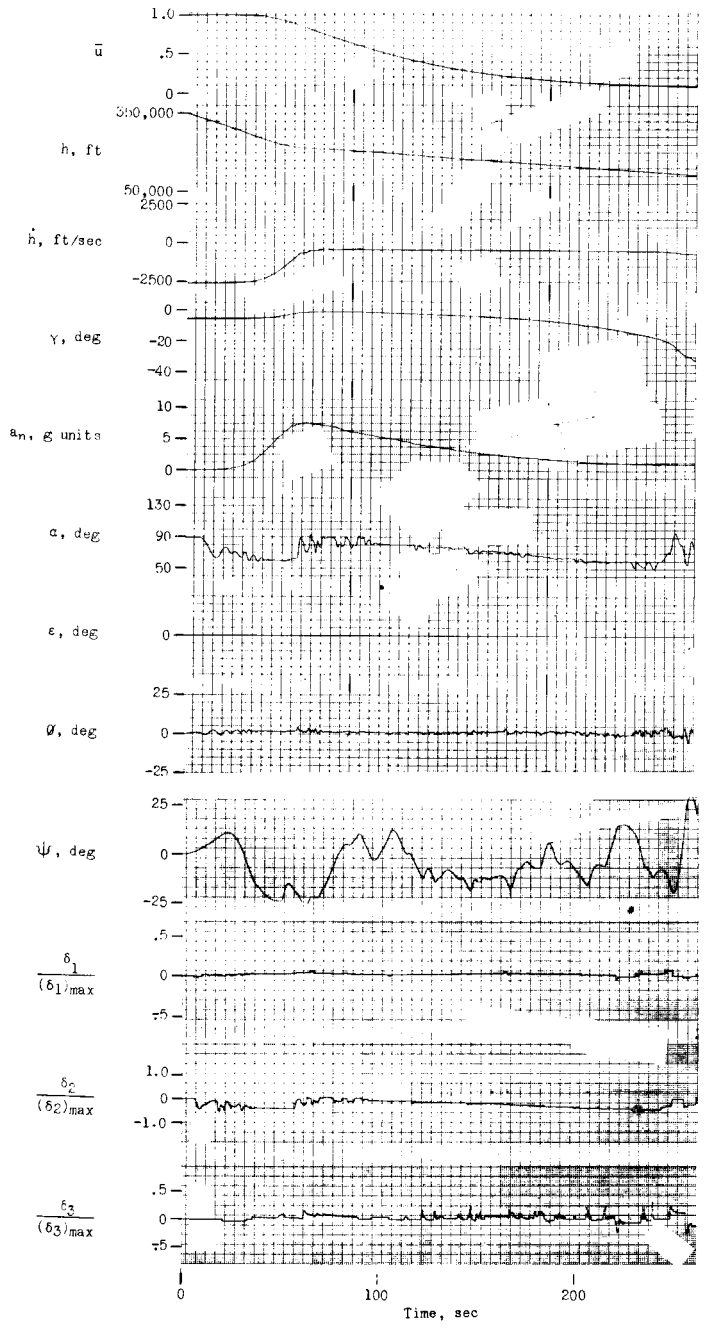

(d) $\gamma_o = -6^o$. Piloting task was to reduce rate of descent to 450 feet per second.

Figure 11.- Concluded.

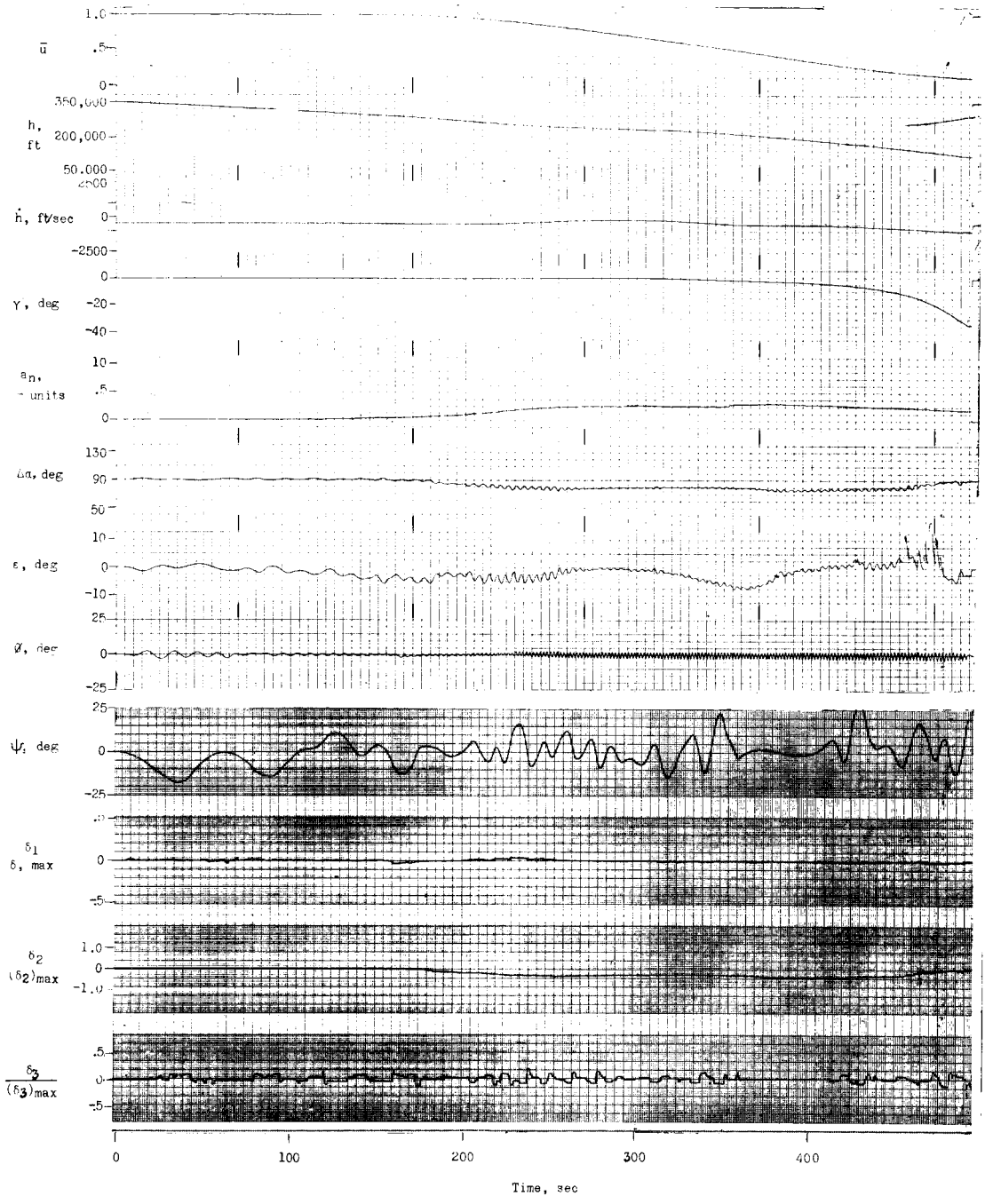

Figure 12.- Simulated entry using finger-tip side-arm controller. Zero damping about all three axes. Piloting task was to maintain zero angle-of-attack error. V_o = 25,863 ft/sec; h_o = 350,000 ft; $\gamma_o = -1^o$.

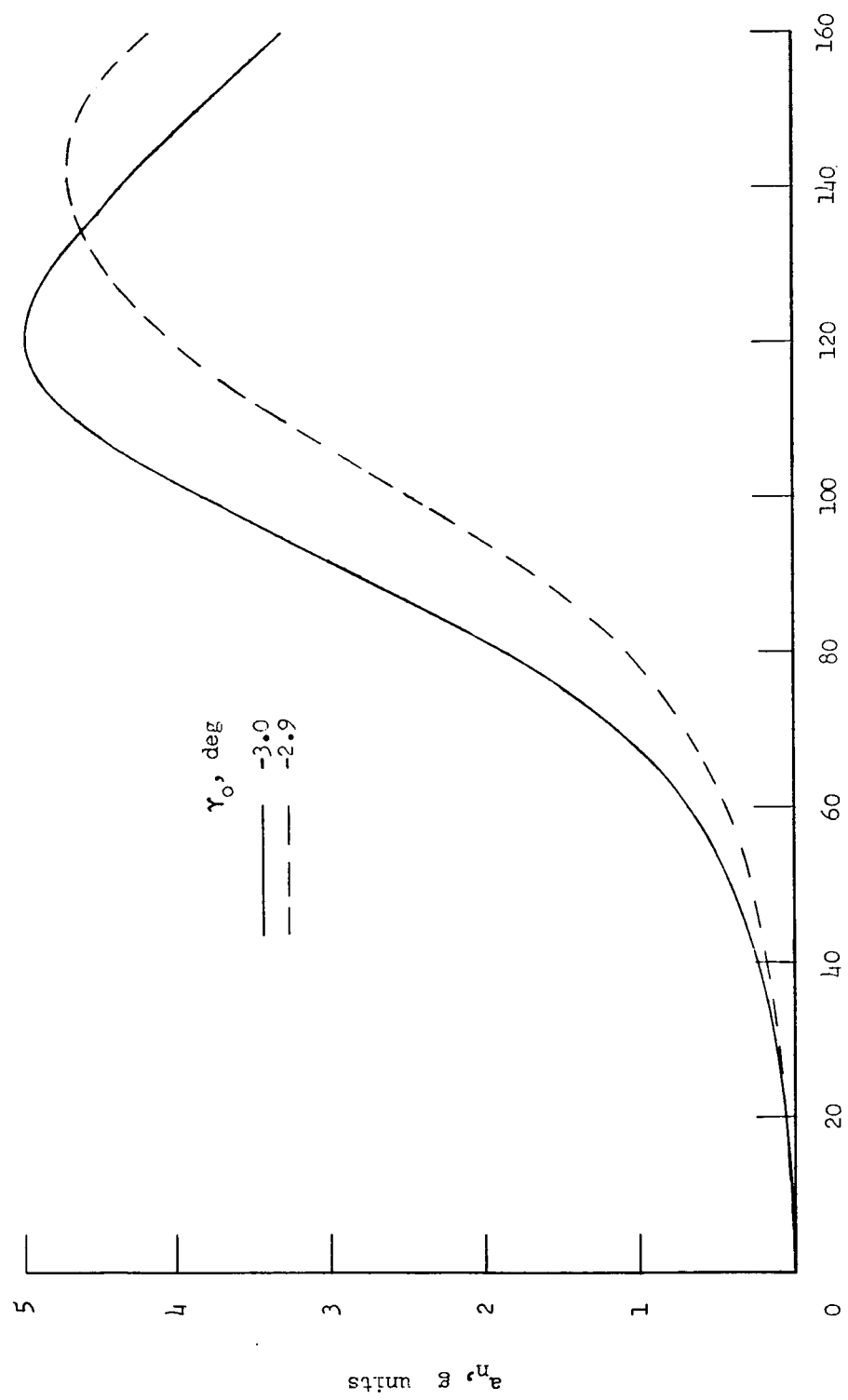

Figure 13.- Effect of small error in entry angle on time history of deceleration. $\alpha = 79°$; $V_o = 25,863$ ft/sec; $h_o = 350,000$ ft.

L-808